Earth-Science Reviews
June 2020, Volume 207, Pages 103218 (23p.)
https://doi.org/10.1016/j.earscirev.2020.103218
https://archimer.ifremer.fr/doc/00632/74383/

Geochemical methods to infer landscape response to Quaternary climate change and land use in depositional archives: A review

Francke Alexander [1, 2, *], Holtvoeth Jens [3], Codilean Alexandru [1, 2, 4], Lacey Jack H. [5], Bayon Germain [6], Dosseto Anthony [1, 2, 4]

[1] Wollongong Isotope Geochronology Laboratory, School of Earth, Atmospheric and Life Sciences, University of Wollongong, Wollongong, NSW, Australia
[2] GeoQuEST Research Centre, School of Earth, Atmosphere, and Life Science, University of Wollongong, Wollongong, NSW, Australia
[3] School of Earth Sciences, University of Bristol, Bristol, United Kingdom
[4] ARC Centre of Excellence for Australian Biodiversity and Heritage (CABAH), University of Wollongong, Wollongong, NSW, Australia
[5] National Environmental Isotope Facility, British Geological Survey, Nottingham, United Kingdom
[6] IFREMER, Marine Geosciences Unit, Brest, France

* Corresponding author : Alexander Francke, email address : afrancke@uow.edu.au

Abstract :

Understanding and quantifying the processes and geochemical cycles associated with catchment erosion, the development of soils and weathering horizons, and terrestrial habitat change beyond the scales of modern observations remain challenging. Such research, however, has become increasingly important to help predict future landscape change in light of increasing land use and rapid global warming. We herein review organic and inorganic geochemical tools applied to depositional archives to better understand various aspects of landscape evolution on geological time scales. We highlight the potentials and limitations of inorganic geochemical analytical methods, such as major element geochemistry, metal and radiogenic isotopes, and in-situ cosmogenic nuclides, as qualitative, semi-quantitative, and quantitative proxies for the transformation of bedrock material via regolith and soils to sediments. We also show how stable isotope geochemistry applied to lacustrine endogenic carbonates can be used to infer rock-water interactions, vegetation change, and soil development in limestone-rich catchments. Proxies focusing on the silicilastic element of sediment formation, transport and deposition are also ideally combined with organic geochemical proxies for vegetation change and soil organic matter evolution in a catchment to gain a comprehensive picture of the Critical Zone's evolution over time. Multi-proxy and multidisciplinary research combining organic and inorganic geochemical techniques from several sedimentary archives in the same catchment have high potential to provide comprehensive information on Quaternary landscape evolution and thus improve the robustness of associated forecasting models.

Keywords : Quaternary landscape evolution, Catchment erosion, Terrestrial habitat change, Land use, Fluvial, Lacustrine, Inorganic geochemistry, Organic geochemistry, Radiogenic isotopes, Metal isotopes, Uranium isotopes, Cosmogenic nuclides

1. Introduction

Geochemical and physical processes forming and modifying the landscape by weathering and erosion play an essential role in controlling atmospheric greenhouse gas concentrations on geological time scales (e.g. Berner 1994). Silicate weathering and carbonate deposition controls the fixation of atmospheric CO_2 in marine sediments (e.g. Gaillardet et al. 1999; Kump et al. 2000). Large tropical and boreal forests as well as permafrost landscapes play a crucial role in biologic greenhouse gas drawdown from the atmosphere. Simultaneously, landscape evolution depends strongly on climate, vegetation, tectonic uplift, and, since the expansion of human settlements and technological advancements, on land use (e.g. Cuéz et al. 2015; Marston 2010; Dotterweich 2008). In the light of anthropogenic climate warming and increasing land use, soils, one of our most important but finite resources, are expected to experience considerable modifications in the near future. Up to 65% of ice-free areas are predicted to be directly affected by climate change, which increases to 80% when the impact of human land use is considered (Ostberg et al. 2018). Deforestation of large forest areas (boreal and tropical) and subsequent accelerated erosion, but also thawing of permafrost landscapes, are frequently an irreversible loss of (biogenic) atmospheric CO_2 sinks. The destruction of such landscapes has consequently been identified as a climate tipping point, i.e. a process that can lead to irreversible warming of the climate system (Lenton et al. 2019).

Studying Quaternary landscapes and (geochemical) processes in the Earth's Critical Zone, (i.e. the near-surface environment, where interactions between rock, soil, air, water, and biota determine the availability of nearly every life-sustaining resource, National Research Council 2001), can help us better understand landscape responses to climate forcing and land use on centennial to millennial time scales where modern observations are not possible. Only geological archives can provide records of long-term trends and/or tipping points of the landscape response and Critical Zone evolution to climate or anthropogenic forcing. Crossing tipping points in landscape evolution can have significant implications for the preservation of soil resources across the globe. This is probably best illustrated by findings from the Balkan Peninsula, where two studies on lake sediment cores have demonstrated that natural and anthropogenic vegetation

changes have controlled threshold-like responses in catchment-wide erosion processes, leaving their trace in the landscape for several millennia (Francke et al. 2019; Rothacker et al. 2018). The study of Quaternary archives has also shown that it may take millennia for landscapes to recover from major modifications (e.g. Holtvoeth et al. 2017), and that anthropogenic changes can make the Critical Zone more sensitive to climate oscillations (Regattieri et al. 2019). Evidence for extensive land use for over two millennia is widespread in Europe, and in particular in the Mediterranean region (Dotterweich 2008). Understanding underlying geochemical cycles and processes is thus crucial for the mitigation of, and adaption to, threshold-like modifications of the Critical Zone. This also applies to parts of the world where substantial human impact could be of shorter duration but higher severity due to technical advancements since the advent of agriculture practises (Dotterweich 2013).

Quantitative modern measurements and modelling of sediment mobilisation and storage are of high importance for understanding soil erosion (see for example the special issue summarised in Panagos and Karoyiannis 2019). Measurements of present day erosion rates provide spatially and temporally highly-resolved data but do not provide insights into the Critical Zone's evolution under unprecedented climate conditions, such rapid climate warming of >2°C as predicted for the near future (IPCC 2014). The amplitude of the landscape's response to such dramatic modifications can only be approximated in geological archives spanning glacial-interglacial transitions (e.g. termination 1 – Last Glacial to Holocene transition; termination 2), and by applying suitable geochemical methods, such as those reviewed herein. Research into the landscape's response to peak warm climate conditions (i.e. similar to those predicted for the next century) is also required. This can be achieved by focusing on past periods with climate conditions similar to the predicted climate conditions, such as MIS5e (marine isotope stage 5e, Eemian), MIS11c and MIS19 (Yin and Berger 2015). Research on Quaternary landscape evolution is thus essential to accurately predict the terrestrial response to a changing future climate, and provide crucial data for the implementation of local, regional, and global (such as IPCC, Intergovernmental Panel on Climate Change) landscape management plans.

Research on Quaternary landscape and Critical Zone evolution usually focuses on depositional archives, such as colluvial deposits, alluvial fans, river (fluvial) sediments, and lacustrine archives, and aims to provide insights into hillslope erosion, land-use impact, and climate change (Dotterweich 2013). Lithological analyses and chronological

work is applied to detect the timing and characteristics of agricultural activity-induced hillslope erosion causing the deposition of colluvium at the footsteps of slopes, enhanced riverbed activity, sediment load transportation, and total sediment flux in a given catchment (e.g. Dotterweich 2008, 2013; Dreibrodt et al. 2010; James 2013). With the advent of novel (bio-)geochemical analytical methods and tools, research on Quaternary landscape evolution now focuses on more quantitative approaches in estimating catchment-wide erosion rates, and on the understanding of (bio-)geochemical cycles and terrestrial habitat change controlled by climate parameters (temperature, amount and seasonality of rainfall) and land use.

Here, we review a variety of new tools to decipher Quaternary landscape and Critical Zone evolution from detrital and non-detrital sedimentary archives using geochemical and biogeochemical methods, and discuss the potential and limitations of these methods. The techniques presented encompass high-resolution geochemical characterisation of continuous to semi-continuous sedimentary archives, using X-ray fluorescence (XRF) core scanning, non-metal (O, C, N) and metal (U, Hf, Nd, Pb) isotope geochemistry, cosmogenic nuclides, and lipid biomarker analysis, (Fig. 1, Table 1). The review is intended to assist the reader in selecting the appropriate analytical methods for studying landscape evolution on geological time scales. This is achieved by providing a comprehensive overview of the potential and limitations of geochemical methods in Quaternary research. The selection of the appropriate analytical method depends not only on the type of the depositional archive (e.g. fluvial, lacustrine) at the study site (Fig. 1, Table 2), but also on the characteristics of the sedimentary archive (such as grain size, mineralogy, sediment composition) and of the catchment (such as bedrock geology, topology).

Fig. 1: Depositional archives and analytical techniques discussed in this review.

2. Sediment chronology and accumulation

The simplest methods to evaluate hillslope erosion in a catchment are qualitative, semi-quantitative, and quantitative assessments on the timing and amount of detrital matter deposition in colluvial, alluvial fans, fluvial and lacustrine deposits (Fig. 1). Colluvial sediments being deposited at foothills of slopes with open vegetation and bare soils (Dreibrodt et al. 2010), alluvial fan deposits as product of gullying evolving upslope (Valentin et al. 2005), and modern and palaeo-fluvial sediments can provide insights

into detrital matter mobility (erosion and river activity) in a given catchment by combining detailed structural and textural investigations with precise chronological work. Chronological information can be inferred from radiocarbon dating (of charcoal, plant remains, pottery artefacts), luminescence dating (of buried medium-sized sediment grains), or archaeological age estimation (Dreibrodt et al. 2010). In particular, colluvial and fluvial deposits benefit from the direct proximity to, and connectivity with, hillslopes and provide a high spatial resolution. However, such records are frequently discontinuous temporally, and occasionally destroyed by ploughing (Dreibrodt et al. 2010). The quality of information on hillslope erosion, as determined from riverbed activity and sediment flux estimates derived from dating of fluvial deposits, depends strongly on site-specific factors, i.e. the connectivity of the landscape and complexity of catchment morphology (Baartman et al. 2013). The same limitations apply for estimates of catchment erosion as derived from detrital matter sediment yields (in $t/km^2/yr$) to a lacustrine basin. Lake sediments, however, benefit from the more continuous, temporally-highly-resolved information provided. For lake basins, the detrital matter sediment yield is difficult to assess since lacustrine sediments are typically composed of a complex mixture of authigenic (such as organic matter or carbonate minerals) and allogenic (detrital matter) components. Zolitschka (1998) modelled total sediment yield using chronological, physical, and (bio-)geochemical proxy analyses to account for non-detrital matter in bulk lacustrine sediment compositions. Firstly, a robust chronology is used to calculate sedimentation rates over time (cm/yr). Physical (density in g/cm^3) and geochemical analyses (such as inorganic and organic carbon contents, biogenic silica contents) of the sediment then allow total sediment accumulation rates to be estimated, as well as individual accumulation rates for organic matter, authigenic/endogenic calcite and biogenic diatoms (mainly diatoms frustules and sponge needles). The detrital matter accumulation rate is then derived from subtracting modelled accumulation rates for non-detrital matter from the total sediment accumulation rate (Zolitschka 1998). Finally, the total sediment yield to the lake can be calculated by normalizing the detrital matter accumulation rate to the catchment size. Estimated sediment yields can be biased by direct aeolian deposition in the lake (resulting in over-estimation), loss of fine-grained detrital matter via outflowing streams (under-estimation), shoreline erosion and mobilisation of lacustrine material by wave action (over-estimation), trapping of coarser material in delta systems (under-estimation), and sediment redistribution in the lake by wind-induced currents and contourite drift (e.g. Martin-Puertas et al. 2012;

Zolitschka 1998; Wennrich et al. 2013; Vogel et al. 2010b). Incomplete supply of detrital matter to the lake and loss of material through outflowing streams can be estimated semi-quantitatively but can vary significantly in different landscapes and over time. Further uncertainties on derived sediment accumulation rates depend on the accuracy of the age-depth relationship in the archive. The chronology of Zolitschka (1998) was based on varve counting, i.e. the number of annually deposited layers in the lake. Varved layers, however, are not available in all sedimentary archives. Age-tie points, for example as derived from tephrochronology and/or radiocarbon dating at low resolution (e.g. Vogel et al. 2010c), might introduce uncertainties to modelled accumulation rates if distributed unevenly across the analysed sequence. This issue can partly be addressed by considering the sediment's lithological features and by using a robust, Bayesian age-depth modelling approach (Blaauw et al. 2018). Alternatively, geochemical techniques can be used to infer catchment erosion rates, as these techniques do not rely on the amount of material deposited in the basin.

3. Inorganic geochemical proxies for catchment erosion, weathering, and terrestrial habitat change

3.1 Element geochemistry as a proxy for erosion and weathering

The advent of X-ray fluorescence (XRF) core scanning techniques over the past decades has made it increasingly fast and efficient to obtain continuous, highly-resolved records of elemental intensities (measured as counts integrated over exposer time of analyses) from sedimentary successions (e.g. Croudace et al. 2006; Croudace et al. 2019a). Elements associated with minerogenic matter (traditionally Al, Si, K, Ti, Fe, Rb, Zr) can be used qualitatively to semi-quantitatively for estimating detrital matter abundances in sedimentary sequences, which is a measure for the amount of detrital material delivered to a sedimentary basin (Davies et al. 2015). The amount of sediment delivered to a lake basin is then often used as qualitative proxy for catchment erosion (e.g. Wennrich et al. 2014; Davies et al. 2015; Francke et al. 2016). Such interpretations can however be biased by mutual dilution with other sedimentary matter deposited at the coring site. Low intensities in siliciclastic-related elements can then for example be controlled by the deposition of more authigenic matter at the coring location, often misleadingly interpreted as less detrital matter supply to the lake and less erosion in the catchment. High-resolution, qualitative to semi-quantitative variability in XRF elemental intensities

is thus ideally supported by quantitative information about the amount of detrital matter in the sediments, which can be modelled (usually at lower resolution) as outlined in section 2. Where quantitative estimates of detrital sediment deposition at the coring site are not available (for example where chronological data are not robust, cf. section 2), the interpretation of elemental intensities as proxy for detrital sediment accumulation is often (qualitatively) evaluated in the light of authigenic matter concentrations and sedimentation rates as inferred from the age-depth model. For example, decreasing K intensities in the sediments of Lake Ohrid (North Macedonia, Albania) during the Early Holocene, are not indicative of decreasing detrital matter supply and reduced catchment erosion (Fig. 2, Francke et al. 2019). Instead, increasing TOC contents (total organic carbon as proxy for the amount of organic matter) and low and steady sedimentation rates imply that decreasing Early Holocene K intensities are rather driven by mutual dilution. Low K intensities during the Mid-Holocene are balanced by moderate TOC and very high TIC (total inorganic carbon as proxy for the amount of endogenic calcite), whilst sedimentation rates are similar to those of the Early Holocene. This might imply that detrital sediment supply to the coring site was decreasing during the Mid-Holocene compared to the Early Holocene (Francke et al. 2019).

Fig. 2: Late Glacial to Holocene (bio-)geochemical proxy data from the sediments of Lake Ohrid (North Macedonia, Albania). Relative variability in TIC (total inorganic carbon as proxy for endogenic calcite), TOC (total organic carbon as proxy for organic matter), K intensities (as proxy for the amount of detrital matter) and sedimentation rates (as inferred from an age-depth model based on tephrochronology) can be used to semi-quantitatively infer the amount of detrital matter supplied to the lake. Detrital matter supply to a lake can be used as proxy for catchment erosion but is ideally supported by quantitative data, which can be modelled as outlined in section 2. Ti/K and the carbon isotope composition of organic matter ($\delta^{13}C_{org}$) are used as proxies for soil development in the catchment (section 3.1 and 3.2). Decreasing soil development during the Late Holocene is a result of increasing human land use and soil degradation. All data from Francke et al. (2019). Carbon isotope analyses was previously conducted at lower resolution by Zanchetta et al. (2018), who also provide proxy interpretation.

Information about the degree of chemical weathering in detrital matter as a measure for soil development in the catchment is usually inferred by normalizing chemically mobile (K, Sr, Ca) to more immobile elements (Ti, Al, Si, Rb, Zr) (Brown 2011; Unkel et al. 2010; Vogel et al. 2015). Ti/K ratios have for example successfully been used as proxy for soil development in the catchment of Lake Ohrid during the Late Glacial to Holocene (Fig. 2, Francke et al. 2019). Decreasing Ti/K ratios in response to Early to Mid-Holocene warming have been interpreted as increasing K mobilisation by chemical weathering in the catchment. The aqueous K is then taken up in the interlayer spaces of phyllosilicates, in interstitial sites of calcite, and adsorbs to clay surfaces and organic matter. Other elemental ratios, such as Rb/Sr, Rb/inc (incoherent scatter), Zr/inc, Zr/Fe, Fe/Si, Fe/Ti have been used as indicators for variations in the particle size diameter in a sediment core. These variations can provide crucial insights into erosion, sediment transport energy, and incision rates in rivers and creeks draining into the lake (Van Daele et al. 2014; Marshall et al. 2011). Extensive analysis of catchment and surface sediment at Lake Towuti have for example revealed that the sediment's Al/Mg ratios in the northern part of the basin are closely related to the kaolinite-to-serpentine ratio. This ratio is controlled by tectonic activity and mass wasting, river incision into the un-weathered, kaolinite-poor, ultramafic bedrock, and grain size (Hasberg et al. 2019; Morlock et al. 2018; Vogel et al. 2015). On geologically short time scales, Al/Mg is then used as proxy for hydrological changes since it responds sensitively to river incision in the catchment and grain size at the drill site, the latter being a measure for shoreline distance and lake level (Morlock et al. 2018; Vogel et al. 2015).

Information about landscape evolution as inferred from elemental intensities and ratios might be biased by a poor connectivity of the catchment (connectivity between hillslope, fluvial system and lake basin), sediment redistribution by lake-internal currents, and the additional deposition of aeolian material as discussed previously (section 2). Interpretations from elemental intensities and ratios need to be evaluated additionally in the light of site-specific settings including bedrock geology and grain size, since changes in sediment source and grain size sorting might impact the geochemical composition of detrital sediments (Kylander et al. 2011; Davies et al. 2015). For example, Ti/K ratios have been used as proxy for the intensity of chemical weathering at lakes Ohrid (North Macedonia, Albania, cf. Fig. 2) and Bourget (France) (Francke et al. 2019; Arnaud et al. 2012), but as an indicator for grain size variability at Lake Tana (Marshall et al. 2011). The site-specific characteristics might even vary between cores

from the same basin if detrital matter is supplied from areas of different bedrock geologies in the same catchment. Interpretations are thus ideally supported by additional proxy analyses and statistical analyses, conducted on a robust set of subsamples from the depositional archive and the source material (weathering horizons and bedrock in the catchment). Additional proxy analyses of depositional archives usually encompass particle size, mineralogical, and/or traditional XRF analyses, whilst catchment samples are analysed for their geochemical and mineralogical properties.

Care has to be taken when interpreting data for elements such as Si, Ca and Sr that occur in both detrital and non-detrital matter. High Si intensities, in particular if normalized to Ti, have been used as indicator for the amount of diatom frustules and/or sponge needles in sediments (Wennrich et al. 2014), whilst other authors used it as a proxy for detrital matter flux or grain size (e.g. Cuven et al. 2010; Vogel et al. 2015). Similarly, Ca and Sr intensities are frequently used as indicators for the amount of calcium carbonate in the sediments (e.g. Vogel et al. 2010a), since Sr has a high affinity to replace Ca in crystal lattices (De Choudens-Sanchez and Gonzalez 2009). At sites with an insufficient supply of dissolved Ca^{2+} and HCO_3^- ions (where carbonate bedrock is scarce or absent), authigenic or endogenic calcium carbonates can be absent in sediments. In such cases, both Ca and Sr may originate from Ca-bearing feldspars, and consequently provide insights into the geochemical composition of detrital matter (e.g. Wennrich et al. 2014; Vogel et al. 2015).

The occurrence of mm-scale detrital laminae in the lithological record can be a useful tool to reconstruct past flood events if they are identified as an indicator of greater hydrodynamic energy of streams draining into the lake (Schillereff et al. 2014). Detecting flood layers in a depositional archive requires highly detailed sedimentological and grain size analyses for differentiation against (tectonic-induced) aerial or subaerial mass wasting and hemi-pelagic background sedimentation (Arnaud et al. 2016). Where flood-related deposition has been confirmed for a specific site, high-resolution records of the frequency and intensity of floods can be established by means of µ-XRF scanning. µ-XRF scanning allows identification of flood layers either by highlighting distinct differences in geochemical composition compared to the hemipelagic background sedimentation, or by providing analyses of grain-size-sensitive elemental ratios, since flood layers are usually associated with coarser grain size distributions (Schillereff et al. 2014). The abundance of flood events is then directly related to the frequency of detected flood layers in the record. Flood intensity can be

inferred either by flood layer thickness or grain size distribution (Arnaud et al. 2016). Determining the particle size (directly or indirectly by µ-XRF scanning) is considered to be the more appropriate approach over measuring the thickness of discrete layers (Lapointe et al. 2012). As for the application of elemental ratios and intensities to hemipelagic sediments, the validity of the palaeoflood record depends strongly on a detailed understanding of lake internal sediment re-distribution processes (Schillereff et al. 2014; Arnaud et al. 2016). For instance, a comparison of two cores from different locations at Lake Allos (Mediterranean French Alps) has shown that hyperpycnal-dominated sites have more complex flood sediment redistribution patterns, requiring the investigation of several cores (Wilhelm et al. 2015). Grain size variability has been proposed as the only suitable method for flood reconstructions at sites dominated by hyperpycnal flows (Wilhelm et al. 2015). Contrastingly, at the second site at Lake Allos, which is dominated by homopycnal flows, deposit thickness could be used as a palaeo-flood indicator, and the analysis of one single core yielded sufficient results.

µ-XRF scanning on palaeoflood records can be applied to wet sediment cores or to resin-impregnated sediment blocks used for thin section preparation (Cuven et al. 2010). XRF on resin-impregnated sediment blocks facilitate for matrix effects resulting from different water contents in wet core samples. The preparation of thin sections from sediment blocks sampled from a core includes freeze-drying and resin saturation under low vacuum, and is therefore relatively time consuming compared to µ-XRF scanning on fresh, wet sediment core surfaces. µ-XRF on resin-impregnated sediment blocks is consequently only useful if it can provide a significant improvement in data quality, or where sediments are poorly consolidated. Other approaches to overcome the problem of poorly consolidated sediments being difficult to analyse with a XRF core scanner, mainly in very young, historical sedimentary successions, includes the recently introduced iBox-FC containment vessel for µ-XRF scanning on freeze cores since it prevents thawing by up to two hours (Gregory et al. 2019).

Additional confidence in the interpretation of elemental intensities and ratios can be gained by calibration methods and comparisons of XRF scanning data to conventional XRF analyses at lower resolution. Several calibration methods have been proposed in the literature, for example by accounting for the sediment's water content (Boyle et al. 2015). If a lower sample resolution (cm to dm resolution) has been identified as sufficient for a given sediment core, discrete, powdered samples can be analysed using an XRF core scanner. This minimizes matrix effects (water content, grain size,

mineralogy) while still making use of a higher cost- and time-efficiency compared to traditional bench top XRF analyses (Profe and Ohlendorf 2019). Univariate and multivariate log-ratio calibration methods have been proposed by Weltje and Tjallingii (2008) and Weltje et al. (2015). Multivariate log-ratio calibrations can provide "absolute" concentrations at a precision similar to those of traditional XRF analyses, but require the analyses of a robust calibration dataset by means of conventional XRF (Weltje et al. 2015). Absolute element concentrations as obtained from XRF scanning can be used for flux or mass-balance calculations at high resolution over time, which is of particular interest for comparisons between several sites (Weltje et al. 2015). The determination of absolute concentrations could even allow the calculation of traditional chemical alteration indices, such as the Chemical Index of Weathering (CIW), the Weathering Index (WI), the Weathering Potential Index (WPI), or the Chemical Index of Alteration (CIA, Price and Velbel 2003; Harnois 1988). These indices essentially measure the degree of depletion between mobile and immobile elements derived from molar mass concentrations of aluminium oxide (Al_2O_3), calcium oxide in silicates (CaO), sodium oxide (Na_2O), and potassium oxide (K_2O). The CIA, for example, is modelled as follows (Nesbitt and Young 1982).

$$CIA=[Al_2O_3/(Al_2O_3+CaO+Na_2O+K_2O)]\times 100 \quad (1)$$

Complications arise from difficulties in accounting for the contributions of detrital, endogenic, and/or authigenic Ca-bearing carbonates, mineral sorting during transportation, and post depositional addition of K due to processes such as illitisation (Goldberg and Humayun 2010). If analyse by core scanning technologies, the application of such indices is still limited since current XRF scanner are not able to detect Na. Elemental ratios are thus still the preferred approach for inferring the degree of chemical alteration in sediments (Arnaud et al. 2016).

3.2 Bulk inorganic carbon isotopes for rock, soil and vegetation interactions

During precipitation of (endogenic) inorganic materials, such as carbonates (e.g. calcite, aragonite) in epilimnetic waters or speleothem, the newly formed mineral captures the relative proportion of ^{12}C and ^{13}C isotopes present in the dissolved inorganic carbon pool ($\delta^{13}C_{DIC}$). This makes endogenic inorganic materials a useful tracer for landscape evolution and an archive of terrestrial environmental change.

For most hard water lakes in limestone catchments, $\delta^{13}C_{DIC}$ can be approximated to the $\delta^{13}C$ of bicarbonate (HCO_3^-), which is the main carbon species present at neutral-alkaline pH. As there is only a minor change in $\delta^{13}C$ during the precipitation of carbonate from lake water (Romanek et al. 1992), the C isotope composition of the mineral phase ($\delta^{13}C_{carb}$) can provide information of past variations in $\delta^{13}C_{DIC}$ (Leng and Marshall 2004). The isotope signal of epilimnetic waters is ideally retrieved from inorganically-precipitated formed carbonates, since biological carbonates (e.g. shell fragments) can be affected by different isotope fractionation processes (vital effects), temperature differences between surface (where endogenic carbonate formation takes place) and bottom waters, the timing of carbonate precipitation, and productivity-controlled stratification of the DIC pool (Leng and Marshall 2004; Lacey et al. 2018). Vital effects might have only limited impact on recorded $\delta^{13}C$ in biogenic carbonates, whilst temperature, timing, and stratification might play a more dominate role (Lacey et al. 2018).

A primary source of DIC in lake water is CO_2 derived from the oxidation of organic matter in terrestrial soils, which is transferred to the lake through surface and groundwater inflows. The $\delta^{13}C$ of DIC supplied to the lake is dependent on the type of photosynthetic metabolism used by the source vegetation (C_3 vs. C_4; see section 4.1). As organic matter accumulates in soils and degrades, CO_2 is produced with a negligible $\delta^{13}C$ offset (Sharp 2007). Following dissolution in superficial waters, the soil-derived CO_2 is hydrated to produce carbonic acid that dissociates, depending on pH, to HCO_3^- with a consistent $\delta^{13}C$ offset from the parent CO_2 (Mook et al. 1974). Therefore, the extent and type of vegetation cover in a catchment, rate of soil development, and amount of CO_2 leaching are primary controls on the availability and $\delta^{13}C$ of soil-derived CO_2. In turn, these variables are driven by palaeoenvironmental and hydroclimate changes, which is a function of oscillations between contrasting glacial and interglacial climates on orbital timescales (Zanchetta et al. 2018). Soil-derived CO_2 may be considered a source of low $\delta^{13}C$ to lake DIC, even when taking into account differences between C_3- and C_4-dominated catchments, in comparison to geological sources of carbon. Supply of soil-derived CO_2 with low $\delta^{13}C$ can also be recorded in the carbon isotope composition of the organic matter pool ($\delta^{13}C_{org}$), if organic material preserved in the sediments is mainly of aquatic origin (Zanchetta et al. 2018). In such a scenario, decreasing $\delta^{13}C$ can be used as an indicator for soil development in the catchment. This has for example been shown for the Late Glacial to Holocene sediments of Lake Ohrid, where the interpretation of $\delta^{13}C_{org}$

is further supported by elemental ratios as inferred by XRF core scanning (cf. section 3.1 and Fig 2, Francke et al., 2019).

Weathering and dissolution of catchment carbonate rocks, typically of a marine affinity, produces significantly higher $\delta^{13}C$ compared to respired soil organic matter (Diefendorf et al. 2008). However, an increased rate of soil respiration lowers the pH of surficial waters and soil-derived CO_2 may be consumed by carbonate dissolution (Jin et al. 2009), thereby buffering any decrease in $\delta^{13}C_{DIC}$ of lake water. Dissolution processes can also impart a threshold behavior for carbonate precipitation in lakes. Catchment soil development, decay, and subsequent CO_2 liberation may be catalysts for the enhanced dissolution of geological carbonates, increasing the supply of Ca^{2+} and HCO_3^- ions to a lake and supporting epilimnetic carbonate precipitation (Lacey et al. 2016).

Whilst the presence of forested catchments, and the associated availability and transfer of soil-derived CO_2 and dissolved geological carbon, are often driven by regional-scale hydroclimate evolution, changes in vegetation cover also affect evapotranspiration. This applies to natural, climate-driven shifts in landscape development and also anthropogenic catchment deforestation (Woodward et al. 2014). A decrease in forest cover and lower evapotranspiration rates may facilitate enhanced water yield from a catchment area and increase the contribution from geological carbon sources with higher $\delta^{13}C$ to lake DIC. In catchments with a constant vegetation assemblage or when considering multi-millennial timescales, as well as in recent sediments, variations in the concentration and $\delta^{13}C$ of atmospheric CO_2 ($\delta^{13}C_{CO2}$) ultimately influences $\delta^{13}C_{DIC}$ via the soil CO_2 leaching-HCO_3^- pathway or by direct exchange with lake water. For extended records that cover several glacial-interglacial cycles, a traceable change in $\delta^{13}C$ of vegetation and subsequent soil-derived CO_2 may be the product of variations in $\delta^{13}C_{CO2}$ assimilated during photosynthesis (Hare et al. 2018). Similar changes have been brought about in recent decades due to the anthropogenic burning of fossil fuels resulting in lower $\delta^{13}C_{CO2}$, which will be reflected in the $\delta^{13}C$ of terrestrial biomass and can be taken into account when interpreting isotope records (Keeling 1979).

Following the transfer and incorporation of soil-derived CO_2 or geological sources of carbon to lake DIC, internal lake processes can act to modify $\delta^{13}C_{DIC}$. Whilst alteration of $\delta^{13}C_{DIC}$ can be the result of natural factors, such as enhanced primary productivity (higher $\delta^{13}C$) or greater recycling of organic matter (lower $\delta^{13}C$), human impact on catchment areas may also drive and exacerbate in-lake modification of $\delta^{13}C_{DIC}$. Agricultural intensification over the 20th century and increased external nutrient loading

on lakes can lead to eutrophication and excess carbon sequestration (Anderson et al. 2014), driving higher $\delta^{13}C_{DIC}$ given the preferential use of ^{12}C by aquatic primary producers. Although the influence of human impact on $\delta^{13}C_{DIC}$ may overprint variations imparted by environmental change, $\delta^{13}C_{DIC}$ may still ultimately be a product of landscape change during anthropogenic modification of catchments. In lakes that are dominated by autochthonous organic matter production, the dependence of $\delta^{13}C_{DIC}$ on catchment-derived soil CO_2 can mean that the presence of terrestrial organic matter components is not necessarily a prerequisite for understanding past landscape change. Past variations in $\delta^{13}C_{carb}$ and $\delta^{13}C_{org}$ in such systems, albeit with a $\delta^{13}C$ offset imparted during photosynthesis, may be positively correlated as both are driven by $\delta^{13}C_{DIC}$ (Zanchetta et al., 2018).

The carbon isotope signal recorded in speleothem archives preserves the same soil development and/or vegetation dependent $\delta^{13}C$ variability as discussed for lake records. The interpretation of speleothem-derived $\delta^{13}C$ records are frequently simplified in comparison to lacustrine archives since previously discussed lake-internal modifications of the desired catchment signal do not apply. Speleothem records furthermore benefit in particular from a high-precision, independent chronology, as derived from uranium-thorium dating. Most non-metal isotope studies applied to speleothem records focus in particular on the recorded hydro-climatic history mainly inferred from oxygen isotope ($\delta^{18}O$) compositions of carbonate minerals (e.g. Bar-Matthews and Ayalon 2004), and carbon isotopes are traditionally an essential part of such studies. The potential of stable carbon isotope compositions of speleothem records as key data for soil stability and pedogenesis has recently been highlighted by Regattieri et al. (2019). The authors report a complex interplay between climate, vegetation development, human land use, and soil erosion in the European Alps during the last 10,000 years, as inferred from $\delta^{13}C$, $\delta^{18}O$, and magnetic susceptibility.

3.3 Metal stable and radiogenic isotopes for erosion and weathering

3.3.1 Uranium isotope activity ratios as indicator for catchment erosion

The activity ratio of uranium isotopes (^{234}U and ^{238}U) in fine-grained detrital matter can provide quantitative estimates of catchment-wide erosion processes (e.g. DePaolo et al. 2006; DePaolo et al. 2012; Dosseto and Schaller 2016; Lee et al. 2010b; Francke et al. 2019; Rothacker et al. 2018; Martin et al. 2019). Mineral grains undergo on-going depletion of ^{234}U, which is measurable in the <63 µm size fraction characterised by a

high surface-to-volume ratio. This depletion occurs by a) direct recoil of ^{234}Th, an intermediate product between ^{238}U and ^{234}U, (b) preferential leaching of ^{234}U embedded in the recoil tracks, and (c) preferential oxidation of ^{234}U compared to ^{238}U (Dosseto et al. 2008; Suresh et al. 2014b, 2013; Ma et al. 2010; Gontier et al. 2015, cf. Fig. 3). Recoil describes the physical displacement of the daughter nuclide (herein: ^{234}Th) during radioactive α-decay (herein of ^{238}U) and can result in the ejection of the daughter nuclide into the surrounding pore space in an open system (Fig. 3). Whilst the decay to ^{234}Th is responsible for the physical displacement, ^{234}U is targeted during isotope analyses for this method since ^{234}Th and ^{234}Pa rapidly decays into ^{234}U (Fig. 3).

Fig. 3: Uranium isotopes (^{234}U and ^{238}U) in fine-grained sediment. Half-lives of ^{238}U, ^{234}U and intermediate nuclides ^{234}Th and ^{234}Pa are also shown. Recoil during the α-decay of *^{238}U to ^{234}Th results in a physical displacement of the daughter nuclide by ~30nm (in most silicates). Half-live for ^{234}Th and ^{234}Pa (hours to days) are not relevant on geological time scales. Loss of ^{234}U occurs mainly in the outer rim of fine-grained (<63µm) detrital grains by recoil of ^{234}Th (and subsequent decay to ^{234}U) or preferential leaching of ^{234}U. Non-detrital matter (organic matter, authigenic and endogenic minerals) are usually enriched in ^{234}U and have to be removed carefully from the bulk sediment prior to analysis. Modified from Martin et al. (2015).*

The (^{234}U/^{238}U) activity ratio of fine-grained sediments (A_{meas}) decreases on geological time scales mainly in response to recoil (process (a)) and is thus a measure of the time elapsed since comminution of the bedrock or coarse (>63µm) regolith (both not showing depletion of ^{234}U) into fine-grained detrital matter, termed *comminution age* (DePaolo et al. 2006; Lee et al. 2010b; Dosseto and Schaller 2016). For a sedimentary deposit, the *sediment residence time* of detrital matter in the catchment (t_{res}, in yr) is the difference between the comminution age and the deposition age, and can be calculated as follows (Francke et al. 2019, Fig. 4):

$$t_{res} = -\frac{1}{\lambda_{234}} \ln \left[\frac{[A_{meas} - (1 - f_{post})] e^{-\lambda_{234} t_{dep}} + (1 - f_{post}) - (1 - f_{pre})}{A_0 - (1 - f_{pre})} \right] \quad (2)$$

with λ_{234} as the ^{234}U decay constant (in yr^{-1}), A_{meas} and A_0 as the measured (^{234}U/^{238}U) activity ratios (unitless) and at time zero (i.e. onset of comminution), and f_{pre} and f_{post} are

the recoil loss factors prior and after to deposition (unitless). The recoil loss factor is the fraction of ^{234}U that is recoiled out of mineral grains. It is calculated as follows (Maher et al. 2006; Kigoshi 1971):

$$f = \frac{1}{4} LS\rho \quad (3)$$

where L is the recoil length of ^{234}Th (30 nm on average in common silicate minerals; Dosseto and Schaller, 2016), ρ the density of the sediment (usually 2.6 g/cm^3), and S the surface area of the sediment (m^2/g) as measured by gas sorption analysis. Thus, in depositional archives where the deposition age is known, it is possible to reconstruct past variations in sediment residence time.

Fig. 4: Conceptual model of detrital matter transit and ^{234}U depletion from source to sink. Depletion of ^{234}U starts in fine-grained detrital matter that is produced as the weathering front on the hillslopes migrates downward over time. Further lowering of the ($^{234}U/^{238}U$) activity ratio occurs in any process related to hillslope and fluvial storage and transport, and during final deposition in a sedimentary basin. The ($^{234}U/^{238}U$) activity ratio can be used to estimate the palaeo-sediment residence times if the time since final deposition is excluded. Modified after Dosseto and Schaller (2016).

The application of U-isotopes as a proxy for catchment erosion requires several considerations (e.g. Dosseto and Schaller 2016; DePaolo et al. 2012). Firstly, authigenic and organic phases need to be eliminated during pre-treatment without altering the outer rim of detrital grains such that the U isotope composition of detrital grains is measured only. Several sequential extraction protocols have been proposed (Suresh et al. 2014a; Martin et al. 2015; DePaolo et al. 2006; Maher et al. 2004; Lee et al. 2010a; Menozzi et al. 2016; Francke et al. 2018). Recently, Francke et al. (2018) have introduced a pre-treatment protocol that allows for the fast processing of large sample sets while meeting the requirements for detrital grain isolation.

The second consideration addresses the initial ($^{234}U/^{238}U$) activity ratios, which is often assumed to be 1, representing secular equilibrium in an un-weathered bedrock. Secular equilibrium is achieved within a time equivalent five times the daughter's half-life. This restricts the application of U isotopes to comminution ages of sediments younger than 1

Ma. Moreover, bedrock often shows ^{238}U-^{234}U disequilibrium even in bedrock older than 1 Ma as a result of deep weathering and fracturing (Handley et al. 2013b; Dosseto and Schaller 2016; Martin et al. 2019). Three potential scenarios have been proposed to address ^{238}U-^{234}U disequilibrium in bedrock material: Firstly, Dosseto and Schaller (2016) argued that the depletion of ^{234}U in source rocks is irrelevant since the isotope ratio is "reset" during comminution as illustrated by glacial outwash measured close to *secular equilibrium* (DePaolo et al. 2012). This implies that an initial activity ratio A_0 of 1 can be used for equation (2). Secondly, Martin et al. (2019) propose that A_0 used in equation (2) can be calculated for a given catchment by accounting for the relative spatial contribution of each rock type and their ($^{234}U/^{238}U$) activity ratios. This requires an a priori knowledge of ($^{234}U/^{238}U$) activity ratios in each rock type, which can be measured for any given catchment on a statistically robust set of bedrock samples or inferred from the literature. Finally, the assumption of an initial activity ratio A_0 of 1 can be relaxed if A_0 is randomly chosen by Monte-Carlo simulations between set values, with the set values being inferred from literature data or direct measurements (Francke et al. 2019).

A third consideration addresses the impact of preferential leaching of ^{234}U on ($^{234}U/^{238}U$) activity ratios of fine-grained detrital matter after comminution. Martin et al. (2019) calculated comminution ages for fluvial sediments in northern Australia based on an formulation introduced by Dosseto and Schaller (2016). This formulation accounts for preferential leaching, thus relaxing the assumption that loss of ^{234}U in fine-grained detrital matter is controlled by recoil only. Sensitivity tests revealed that estimated comminution ages depend in particular on the chosen ^{238}U leaching rate (Martin et al. 2019). Using the formulation to account for preferential leaching, however, resulted in poor correlations between sediment residence times, vegetation cover, and annual rainfall, which were otherwise evident if not accounting for preferential leaching (loss of ^{234}U by recoil only). This can probably be attributed to a complete dissolution of the weathering-active surface on geologically short time scales (Li et al. 2018). This implies that measured ($^{234}U/^{238}U$) activity ratios of fine-grained detrital matter reflect the recoil-induced loss of ^{234}U from the weathering-inactive mineral surface only, and that preferential leaching is insignificant for the comminution dating approach (Li et al. 2018).

The fourth consideration addresses the requirement of accurate determination of the recoil loss fraction f (equation 3). Because there is a two-order magnitude difference

between the length scale of ^{234}Th recoil and the length of the molecule N_2 (0.354 nm) used for surface area quantification, the estimated the recoil loss fraction using gas sorption analysis can result in an overestimation of the surface area relevant to ^{234}Th recoil. To address this difference, a fractal correction has been proposed (Bourdon et al., 2019). Francke et al. (2018) have shown, however, that the fractal correction should only be applied if micro- (<2 nm) or/and meso-pores (2-50 nm) are present in the sediments, which can be assessed during gas sorption analysis. Gas sorption analysis of selected fluvial sediments from northern Australia (Martin et al. 2019) and lacustrine sediments from Lake Ohrid in the Mediterranean (Francke et al. 2019) has shown that both scenarios (i.e. presence or absence of micro- and meso-pores) are possible, and the assessment of whether a fractal correction is necessary has to be undertaken for each study.

The comminution dating approach assumes a constant recoil loss fraction since comminution, i.e. before and after final deposition. Further considerations have recently been made to address the possibility that the recoil loss fraction after final deposition may be different than that during sediment transport throughout the catchment. Loss of ^{234}U could be significantly inhibited in densely compacted sediments with small pore space, where ^{234}Th could be recoiled from one grain into another and is thus not lost from sediments (Francke et al. 2019). Whilst such considerations are probably not significant for relatively unconsolidated modern stream samples and for Late Glacial to Holocene deposits (Francke et al. 2019), a reduced loss of recoiled ^{234}Th after deposition in marine or lacustrine sediment cores at greater depths could result in a significant underestimation of calculated catchment *sediment residence times*. Equation (2) allows accounting for different recoil loss fractions before and after final deposition enabling the assessment of loss in ^{234}Th after final deposition in future studies focusing on older time intervals.

The use of U isotopes to infer *sediment residence times*, sometimes referred as *comminution dating* was first applied to a marine sediment core and revealed that the provenance of the clastic matter deposited in the North Atlantic might have changed dramatically on glacial-interglacial time scales between Iceland and northern Europe (DePaolo et al., 2006). The inferred variability in *comminution ages* was thereby attributed to changing sediment sources. During glacial periods, the sediments were dominated by material being previously stored in soils, continental shelves, or elsewhere on the seafloor. Supply of young sediment sourcing from Iceland during

interglacial periods results in lower *comminution ages*, i.e. *shorter sediment residence times*. Since then, comminution dating has mainly been applied to fluvial environments in Australia, China and California (Dosseto et al. 2010; Handley et al. 2013a; Lee et al. 2010b; Martin et al. 2019; Li et al. 2017). This has provided insights about catchment-wide erosion processes in response to vegetation cover and climate parameters on modern to geological time scales.

Martin et al. (2019) reported moderate to strong correlations of ($^{234}U/^{238}U$) activity ratios in modern stream samples from the Gulf of Carpentaria (northern Australia) to annual and seasonal distribution of rainfall, and to vegetation cover in the catchment. ($^{234}U/^{238}U$) activity ratios of modern stream samples from China have been reported to show an excellent agreement to previously published erosion rates as inferred from cosmogenic nuclides (Li et al. 2017). Palaeo-channel sediments samples in SE Australia show a strong correspondence to glacial-interglacial climate variability, which has been attributed to erosion of young upland soils during glacial periods and re-working of old fluvial sediments during interglacials (Dosseto et al. 2010). Comprehensive multi-proxy studies using the ($^{234}U/^{238}U$) activity ratio alongside traditional palaeoclimate and palynological proxy data have been conducted on two Late Glacial to Holocene lacustrine sediment sequences from the Balkan Peninsula (Francke et al. 2019; Rothacker et al. 2018, lakes Ohrid and Dojran). These lakes drain small catchments (1002 km^2 for Lake Ohrid and 275 km^2 for Lake Dojran). Whilst in large catchments (~>1 × 10^6 km^2), the ($^{234}U/^{238}U$) activity ratio can be modified during fluvial transport and storage (Dosseto et al. 2010; Martin et al. 2019), the sediment residence time in the small catchments that lack significant lateral channel migration mainly reflects hillslope storage. Since the weathering front moves downwards over time, the residence time should decreases with increasing depth in weathering profiles (e.g. Suresh et al. 2013). Consequently in small catchments where fluvial storage is negligible, variations in sediment residence time in depositional archives can reflect changes in hillslope erosion depth over time (Rothacker et al. 2018; Francke et al. 2019). It is thus possible to assess changes in the type of erosion processes, such as deep gullying or mass wasting versus shallow sheet wash, and how these variations relate to changes in vegetation cover and climatic conditions. At Lake Ohrid in North Macedonia and Albania, Late Glacial to Holocene *palaeo-sediment residence times* and catchment erosion is strongly controlled by climate conditions during the Late Glacial and Early Holocene (Francke et al. 2019, Fig. 5). Shallow erosion of thick soils (long *palaeo-sediment residence time)* prevails

during cold and dry climates (Late Glacial, Younger Dryas), and deep erosion of thin soils (short *palaeo-sediment residence time)* persists during wet and warm intervals (Bølling/Allerød, Early Holocene). The expansion of a dense vegetation cover, as indicated by tree-versus-herb pollen percentages >90% (Fig. 5B, C), suggests that a threshold is crossed in catchment erosion processes during the Early to Mid-Holocene transition. Dense woodland vegetation expanding to high elevations prevents the erosion of thin soils by deep erosion in response to climate forcing. These outcomes display in particular how changes in vegetation cover can impart a threshold-like response in catchment erosion to climate variablity, information that is crucial in the light of increasing anthropogenic deforestation and climate warming.

Fig. 5: ***A:*** *Late Glacial to Holocene palaeo-sediment residence times and tree versus herb pollen percentages from Lake Ohrid (Francke et al. 2019). YD: Younger Dryas, B/A = Bølling/Allerød. Cold and dry intervals highlighted in blue are derived from Francke et al. (2019). Grey bar indicates tree-versus-herb pollen percentages >90% indicating the expansion of dense woodland vegetation at all elevations in the catchment.* ***B:*** *Profile across the catchment of Lake Ohrid and conceptual model of Late Glacial to Holocene catchment erosion showcasing how the expansion of dense woodland vegetation restricts deep erosion of thin soils at high elevation since the Early to Mid-Holocene transition. Thus, as the vegetation cover becomes dominated by trees, climate variability has a more muted role on catchment erosion (compared to the Late Pleistocene and Early Holocene). Modified from Francke et al. (2019).*

3.3.2 Hafnium (Hf), neodymium (Nd) and lead (Pb) isotopes as indicators for sediment source and weathering

The application of radiogenic isotopes to sedimentary records can provide information on both sediment provenance and the degree of silicate weathering in corresponding soils, which, taken together, can be used to disentangle the impact of climate change and human activities on landscapes. To a first approximation, radiogenic isotope compositions of detrital sediments are mainly set by the parent-daughter ratios and the mean age of the source rocks (e.g. Banner 2004). Compared to other geochemical tracers, neodymium (Nd) isotopes are unique in the sense that their isotopic composition remains mostly unchanged during continental weathering and sediment transport (e.g. Goldstein and Jacobsen 1988). This particularity can be used to

fingerprint sediment sources and quantify terrigenous fluxes, which help identifying recent periods of enhanced erosion related to land use (e.g. Wan et al. 2015; Giosan et al. 2017; Chatterjee and Ray 2017; Bayon et al. 2019). In contrast to Nd, the distribution of Hf and Pb isotopes in detrital sediments is also controlled by weathering and mineral sorting effects. The grain-size and weathering dependence of Hf and Pb isotopic ratios in sediments reflects the strong decoupling of corresponding parent-daughter elements (i.e. Lu-Hf and U-Th-Pb) during magmatic processes. The relatively large degree of fractionation between Lu and Hf and U-Th and Pb during magmatic crystallization results, with time and radioactive decay of ^{176}Lu to ^{176}Hf and U-series, to markedly different radiogenic isotope compositions in minerals (Banner 2004; Blum and Erel 2003). Because weathering does not affect rocks uniformly, these characteristics provide a mean for investigating silicate weathering processes in soils and detrital sediments (Blum and Erel 1995; Aubert et al. 2001; Bayon et al. 2016; Harlavan et al. 1998). Over recent years, this principle was applied to marine sediment records recovered off the Congo River, in which a particular sediment horizon is associated with the export of clays with distinctively high Al/K ratios and radiogenic Hf isotopic signatures, indicative of more intense weathering conditions in the watershed (Bayon et al. 2019; Bayon et al. 2012). Because the timing of sediment deposition, around 2500 years ago, coincided with the widespread migration of Bantu-speaking peoples across Central Africa, these particular geochemical signatures were partly linked to the intensification of human activities and enhanced soil erosion in the rainforest at that time. Similarly, Fontanier et al. (2018) also documented a sudden increase in radiogenic Hf signatures in the upper part of a sediment core offshore north-western Madagascar, interpreted as the result of intensifying weathering due to enhanced land use and deforestation over the last 60 years. As emphasized by these examples, silicate weathering can respond rapidly, within a few decades only, to major climatic and/or anthropogenic disturbances on continents.

In addition to detrital sediments, authigenic mineral phases such as iron (Fe) oxides can be also used in sediment records as archives of past weathering and/or anthropogenic activities. Iron oxides form directly in soils upon chemical weathering, being subsequently transported as suspended particulates in rivers prior to deposition as sediments (Bayon et al. 2009). Authigenic Fe oxide phases also commonly precipitate from water in the ocean, rivers and lakes, concentrating substantial amounts of dissolved trace elements such as Nd, Hf and Pb, initially released during weathering

processes or from anthropogenic pollution sources (Boyle et al. 1977; Süfke et al. 2019). A recent investigation of Fe-oxides extracted from sediments deposited in a lake in Switzerland reported a trend towards suddenly increasing radiogenic Pb signatures from ~2200 cal. years B.P., departing from the natural weathering signal of the earlier Holocene period (Süfke et al. 2019). This abrupt change of the Pb isotopic composition of Fe-oxides coincided exactly with the rise of the Roman Empire and intensifications of mining activity all over Europe, hence suggesting that it corresponded to an atmospheric Pb pollution signature, in agreement with earlier studies (Renberg et al. 2002). All the examples listed above clearly show the utility of radiogenic isotopes and other weathering proxies in studies aiming to investigate the impact of humans on the environment.

3.4 In-situ cosmogenic nuclide analysis for catchment erosion

Several of the *in situ* cosmogenic nuclides, including the stable ^{3}He and ^{21}Ne, and the radioactive ^{10}Be, ^{14}C, ^{26}Al, and ^{36}Cl, are now routinely measured and have been used in geomorphological studies for the last three decades (Dunai 2010; Granger and Schaller 2014; Bierman 2004). Of these nuclides, however, ^{10}Be (T1/2=1.387 Myr, Chmeleff et al. 2010; Korschinek et al. 2010) produced in quartz is the 'workhorse' for *in situ* applications, and the majority of *in situ* cosmogenic nuclide studies have used ^{10}Be, either alone or in conjunction with other cosmogenic nuclides such as ^{26}Al, ^{21}Ne, and ^{14}C. Given the long half-life of ^{10}Be and the increasingly low analytical backgrounds that can be realized (Wilcken et al. 2019), it is now possible to analyse samples covering a wide range of temporal settings, including historic times (Schaefer et al. 2009). The rate at which cosmogenic nuclides are produced is extremely low – a couple of atoms per gram of rock per year (Borchers et al. 2016) – and the rapid attenuation of cosmic radiation with depth (Fig. 6) confines the production of cosmogenic nuclides to the upper few meters of the crust, the production rate decreasing roughly exponentially with depth (Argento et al. 2015a, b). Production rates of cosmogenic nuclides are mainly a function of geomagnetic latitude and altitude above sea level (Balco et al. 2008; Lifton et al. 2014). Site-specific production rates are also subject to several other factors, such as the geometry of the surrounding topography, which shields part of the incoming cosmic radiation (Dunne et al. 1999; Codilean 2006; DiBiase 2018).

Fig. 6: Production rates of in situ ^{10}Be in quartz as a function of depth. Note how the production rate by high-energy neutrons (spallation), although substantially higher at the surface than that by muons, attenuates more quickly with depth. This means that whereas in the upper few metres of rock, spallation reactions are dominant, at greater depths, muons account for the production of virtually all ^{10}Be. Modified from Dunai (2010) and based on Heisinger et al. (2002a,b).

The application of cosmogenic nuclides to the study of sedimentary archives is based on two principles: (i) cosmogenic nuclide concentrations are directly proportional to the exposure time to cosmic radiation – i.e., nuclides accumulate in surficial deposits over time such that their concentration will be directly related not only to the exposure age but also to the rate at which the surface is eroding (Granger and Schaller 2014), and (ii) two radionuclides will be produced at a fixed ratio but will decay at different rates dictated by their half-lives (Granger and Smith 2000; Granger and Muzikar 2001) – i.e., when previously exposed river sediment becomes temporarily or permanently shielded from cosmic radiation, the differential decay of two cosmogenic radionuclides results in a change in the ratio of these nuclides in proportion to the duration of burial. Given that the majority of cosmogenic nuclide studies have used ^{10}Be for exposure dating and quantifying denudation rates, and the ^{10}Be – ^{26}Al pair for burial dating, we refer to these nuclides in the following sections. However, the principles discussed below apply to all in-situ produced cosmogenic nuclides.

3.4.1 Quantifying basin wide denudation rates

As a parcel of rock or sediment is brought toward the surface by erosion on a hillslope, its ^{10}Be concentration (N) increases at a rate that depends mainly on the rate of erosion (ε), and the ^{10}Be surface production rate ($P(0)$) at that locality. The temporal evolution of the ^{10}Be concentration in this parcel is accurately described by (Lal 1991; Dunai 2010):

$$N(z,t) = \sum_{i=1}^{n} \frac{P(0)_i}{\lambda + \rho\varepsilon/\Lambda_i} e^{-\rho(z_o - \varepsilon t)/\Lambda_i} \left[1 - e^{-(\lambda + \rho\varepsilon/\Lambda_i)t}\right] \quad (4)$$

where λ is the ^{10}Be decay constant, z_o is the initial depth beneath the surface [cm], t is exposure time [yr], ρ is the density of the eroded material [g.cm^{-3}] and $P(0)_i$ and Λ_i are

the surface ^{10}Be production rate [atoms.g^{-1}.yr^{-1}] and the mean cosmic ray attenuation length with depth [g.cm^{-2}] for a given production pathway, respectively (Granger and Smith 2000). Over sufficiently long periods of time ($T \gg 1/(\lambda + \rho\varepsilon/\Lambda_i)$), the ^{10}Be concentration in the parcel is no longer time dependent, rather it is determined by the erosion rate alone (Fig 7). Under these steady-state conditions, equation (4) reduces to:

$$N = \sum_{i=1}^{n} \frac{P(0)_i}{\lambda + \rho\varepsilon/\Lambda_i} \qquad (5)$$

One of the most important prerequisites for equation (5) to be valid is that erosion is continuous, occurring by grain-by-grain removal of material, and that it is not episodic, occurring by the spontaneous removal of discrete blocks of varying thicknesses.

Fig. 7: Temporal evolution of the surface ^{10}Be concentration under continuous (left) and episodic (right) erosion regimes. Under continuous erosion the surface ^{10}Be concentration reaches a constant value (red curve), and the amount of ^{10}Be produced by cosmic rays will equal the amount removed by erosion and radioactive decay. Episodic erosion processes, on the other hand, remove discrete blocks of rock or sediment. The truncation of the exponentially decreasing ^{10}Be depth-profile (blue curve) means that a constant surface ^{10}Be concentration will not be reached; instead this will fluctuate with time as the amount of ^{10}Be produced will never match the amount removed by erosion. (1) If the removal of blocks is periodic (time between spalling events T_i = constant = T) and the size of the blocks is uniform (w constant) the ^{10}Be concentration will fluctuate around a long-term average value (Small et al. 1997). (2) If the removal of blocks follows a Poisson process, with both T_i and w being stochastic variables, the average ^{10}Be concentration and its spread will depend on T (the average time between spalling events) and the probability distribution of w (Muzikar 2008, 2009).

When the parcel of rock or sediment reaches the surface, it is transported via hillslope processes to the fluvial system, where it mixes with sediment from other parts of the contributing basin. Thus, rivers act not only as agents of erosion but also as integrators, collecting sediment from all parts of the basin in an amount that is proportional to their denudation rates such that the sediment will contain an average concentration of ^{10}Be at the outlet of the basin that is a measure of the basin's mean denudation rate. If (i) the

volume of sediment contributed by different parts of the basin is proportional to the area of those parts, and (ii) the averaging timescale of denudation in the basin is short relative to the ^{10}Be half-life (or that of the nuclide of choice), and (iii) the timescale of sediment transport and storage is negligible as compared to the timescale of denudation (Brown et al. 1995; Bierman and Steig 1996; Granger et al. 1996), then equation (5) can also be used to calculate basin-wide average denudation rates ($\bar{e}$) from the average ^{10}Be concentration of the mix of sediment leaving a basin ($\bar{N}$).

Cosmogenic nuclide-based denudation rates have now been determined in more than 4000 basins world-wide (Codilean et al. 2018), contributing substantially to our understanding of the relative effects of climate and topography on denudation rates in a wide range of tectonic settings (Granger and Schaller 2014). However, there is still a paucity of data from landscapes situated at the extremes of denudation-rate and topography spectra, confounding studies aiming to infer global-scale trends from compilations of ^{10}Be-based denudation rates (Portenga and Bierman 2011; Willenbring et al. 2013; Harel et al. 2016). At one end of the spectrum are the low-gradient arid landscapes that occupy large portions of Gondwana remnants such as Australia, Africa, and South America. Here lithology plays a key role in controlling landform morphology and thus the styles and rates of hillslope evolution, and therefore also cosmogenic nuclide inventories (Cazes et al. 2020). The low gradients also mean that sediment may spend prolonged periods of time (on the order of 10^5-10^6 years) within hillslope soils (Struck et al. 2018a; Makhubela et al. 2019) or moving through the fluvial network (Struck et al. 2018b). Both cases may lead to increased ^{10}Be inventories and thus underestimated denudation rates, and potentially to the alteration of any source area environmental signals travelling from source to sink (Fülöp et al. in press). At the other end of the spectrum are the steep (and often wet) tectonically active landscapes where episodic erosion processes such as landsliding are the most important means of delivering sediment from hillslopes to the drainage network (Korup et al. 2010).

Episodic erosion processes remove discrete blocks of rock or sediment, and the truncation of the exponentially decreasing ^{10}Be depth-profile (Fig. 6) means that a constant surface ^{10}Be concentration will not be reached (Fig. 7). Instead the ^{10}Be concentration will follow a time independent, equilibrium statistical distribution ($f_{eq}(N)$) that depends on the magnitude distribution and the recurrence interval of the

episodic erosion process (Muzikar 2008, 2009, 2019). For this equilibrium condition, the average ^{10}Be concentration on a hillslope ($\langle N \rangle$) is given by Muzikar (2009):

$$\langle N \rangle = \int_0^\infty dN f_{eq}(N) N = \frac{P(0)}{\lambda + 1/T\left(1 - \overline{e^{-\rho w/\Lambda}}\right)} \quad (6)$$

where T is the average time between landslides (or other episodic spalling events) and w is the thickness of the removed block, a stochastic variable governed by a distribution $g(w)$. The notation $\overline{e^{-\rho w/\Lambda}}$ stands for an average over the thickness distribution $g(w)$:

$$\overline{e^{-\rho w/\Lambda}} = \int_0^\infty dw g(w) e^{-\rho w/\Lambda} \quad (7)$$

The mean square fluctuation in N (i.e., the likely spread in ^{10}Be concentrations) is given by Muzikar (2009):

$$\langle (\Delta N)^2 \rangle = \langle N^2 \rangle - \langle N \rangle^2 = \langle N \rangle \left(\frac{2P(0)T}{1 + 2T\lambda - \overline{e^{-2\rho w/\Lambda}}} - \langle N \rangle \right) \quad (8)$$

The brackets $\langle\ \rangle$ in equations (6) and (8) stand for an average over time. Therefore, $\langle N \rangle$ and $\langle (\Delta N)^2 \rangle$ represent the average ^{10}Be concentration and the likely spread in this concentration, respectively, observed on a hillslope, or at the outlet of a catchment, over a period of time. Equations (6) and (8) can be applied to a wide range of episodic surface erosion scenarios that follow a Poisson process (for more extreme scenarios see Muzikar 2019). The essential point is that if the magnitude-frequency distribution of landslides in a given catchment is known independently, equations (6) and (8) can be used to determine the long-term average and the spread in ^{10}Be concentrations in the sediment leaving this catchment. Conversely, if the long-term average and the spread in ^{10}Be concentrations in the exported sediment are known, equations (6) and (8) can also be applied to gain insights to links with the size distribution of landslides, and their recurrence intervals.

Improvements in sample measurement (Wilcken et al. 2019) and enhanced sample throughput will enable the large number of sample counts necessary to go beyond mean denudation rates of large catchments in the future. Delving deeper into the processes

controlling sediment production and sediment transport at the catchment scale could be achieved by looking at, for example, single-clast distributions of cosmogenic nuclide concentrations (Codilean et al. 2008; McPhillips et al. 2014; Carretier et al. 2019; Muzikar 2019; Prush and Oskin 2020). The applications of meteoric ^{10}Be (e.g. Dannhaus et al. 2018) and applications of in-situ produced ^{10}Be in minerals other than quartz (e.g. Moore and Granger 2019) will also extend the applicability of basin-wide denudation rate studies to non-quartz bearing lithologies.

3.4.2 Dating of sedimentary deposits and quantifying palaeo-denudation rates

As shown in Fig. 6, cosmogenic nuclide production rates decrease roughly exponentially with depth, and this property has been exploited as a means of dating the abandonment of fluvial deposits (Anderson et al. 1996; Repka et al. 1997). The principle behind this application is illustrated in Fig. 8, and is explained as follows. Clasts building up a fluvial deposit arrive at the site with varying cosmogenic nuclide concentrations (fuzzy blue band in Fig. 8) but are assumed to have been emplaced with uniform distribution of nuclide concentrations with depth ($^{10}Be(in)$). Due to the exponential decrease in production rate with depth, subsequent accumulation of cosmogenic nuclides will result in a shift from the original uniform distribution to one following an exponentially decaying curve. Mean nuclide concentrations measured from amalgamated clasts taken at the surface ($^{10}Be(s1)$) and subsurface ($^{10}Be(s2)$) of the deposit will differ from each other in proportion to the amount of time elapsed since terrace abandonment. Thus, provided that the subsurface sample is deep enough relative to the mean cosmic ray attenuation length (see above), the depositional age of the terrace is simply given by $^{10}Be(s1) - {}^{10}Be(s2)$. In addition, the basin-wide denudation rate at the time of terrace emplacement (i.e., palaeo-denudation rate) can also be calculated using $^{10}Be(s2)$. The technique relies on a couple of assumptions (Anderson et al., 1996): (i) clasts are emplaced with uniform distribution of nuclide concentrations with depth, (ii) the deposit has not been disturbed or mixed since emplacement (e.g. by bioturbation, cryoturbation, pedogenesis, etc.), and (iii) the terrace surface has not been modified, either by subsequent erosion or deposition, since emplacement. In most cases these assumptions are impossible to test *a priori*, and a successful application of the technique involves the collection of several samples (e.g., n > 10) from a depth profile that is a couple of meters in depth, and the use of numerical approaches that allow for

complicating factors such as vertical mixing post deposition, varying inheritance with depth, erosion of the terrace surface, etc., to be explicitly considered (Hidy et al. 2010).

Fig. 8: Principles of using cosmogenic nuclide depth profiles for dating fluvial deposits (modified after Anderson et al. 1996). See text for more details.

Deposits can also be dated using a pair of cosmogenic radionuclides (or a pair consisting of one radionuclide and one stable nuclide) by exploiting the property that these nuclides are produced at a fixed ratio but have different half-lives (Fig. 9), as long as the deposit is old relative to the nuclide pair's half-lives. The differential decay rates can then be used to infer the time elapsed since burial (Granger and Smith 2000; Granger and Muzikar 2001). The most common nuclide pair used in burial dating is ^{26}Al and ^{10}Be, with a production ratio of Al/Be = ~6.75 and with half-lives of 0.7 Myr and 1.39 Myr, respectively. Upon burial and cessation of nuclide production, the differential decay of the two nuclides results in a change in the ratio of these nuclides (Fig. 9A), and the burial age can be calculated as:

$$t_b = -\ln\left(\frac{R_{AB}(t_b)}{R_{AB}(t_0)}\right)\Big/(\lambda_A - \lambda_B) \qquad (9)$$

where t_b is the burial duration (years) , λ_A and λ_B are the half-lives of the two nuclides, and $R_{AB}(t_b)$ and $R_{AB}(t_0)$ are the measured and production ratios of the nuclide pair, respectively (Fig 9A). The useful age range of a burial dating nuclide pair is set by the half-lives of the two nuclides; at some point the nuclide with the shorter half-life attains a concentration where measurement is no longer possible. Under ideal conditions, the useful range of the ^{26}Al and ^{10}Be pair is between 0.5 - 6 Myr (Granger 2006). This range can be extended, however by introducing a third nuclide, ^{21}Ne, that is stable. Because ^{10}Be has a half-life that is nearly double that of ^{26}Al, and because ^{10}Be can be measured more precisely at low concentrations than ^{26}Al, the useful range of the ^{10}Be–^{21}Ne burial dating pair is more than double that of the ^{26}Al–^{10}Be pair. Thus, ^{10}Be–^{21}Ne burial dating should be applicable even for deposits of Miocene age (Balco and Shuster 2009).

Fig. 9: Diagrams illustrating the principles of burial dating. (A) Fast and complete burial. During exposure to cosmic radiation the ratio of a nuclide pair (such as ^{26}Al and ^{10}Be)

evolves such that the sample will plot inside the erosion island. Upon burial and cessation of nuclide production, the ratio of the nuclide pair will start to decrease following the path indicated by the red arrow. This ratio is proportional to the duration of burial and thus can be used to calculate the burial age of the sample. The position of the sample in the Al/Be vs. Be space also provides information on the pre-burial denudation rate. (B) Incomplete burial with variable inheritance. Samples that were subject to a simple and complete burial history will rotate along trends indicated by the blue lines. Samples with variable inheritance (red circles) but similar post burial production will evolve on displaced lines (red lines), parallel to the trends indicated by the blue lines. The slope of the trend defined by the samples is used to calculate the burial age. Modified from Dunai (2010) and based on Granger and Muzikar (2001) and Balco and Rovey (2008).

The method outlined above is ideal for dating thick sedimentary deposits or cave sediments. However, in many cases, post-burial production of cosmogenic nuclides due to muons or as a result of intervals of re-exposure, must be taken into account (Fig. 9B). The variation in measured ^{26}Al and ^{10}Be (or ^{21}Ne and ^{10}Be) in a group of samples collected from the same stratigraphic layer can be used to solve explicitly for the post-burial component that will be common among the samples. This method, called isochron burial dating (Balco and Rovey 2008) was successfully applied to dating of poorly preserved fluvial terraces as old as ~4 Myr (Erlanger et al. 2012).

4. Organic geochemical proxies for terrestrial habitat change

As vegetation adapts to climate fluctuations or is modified or replaced through human activities, the molecular composition of plant litter and soil organic matter exported towards a depositional environmental archive changes accordingly. Molecules of known biological origin (biomarkers) or their chemical properties such as the carbon isotope ratio (^{13}C/^{12}C) can be used to reconstruct such changes even if macro- or microscopically identifiable fossil material is absent due to continuous particle break-up during transport. The aboveground vegetation typically represents the smaller part of the terrestrial organic carbon pool. In undisturbed ecosystems, degrading plant litter and belowground biomass consisting of root tissue represent the larger part, in fact, two-thirds of the global terrestrial organic carbon is stored in soils (Post et al. 1982). The dynamics of the soil carbon pool can differ substantially in their response to environmental change, with slow build-up of the soil carbon pool resulting in lead-lag

relationships with climatic parameters or vegetation, for example. In lacustrine catchments, lake level fluctuations can introduce an additional level of complexity. Changes in lake surface area inversely affect the surface area occupied by the surrounding terrestrial habitats and modify the fluxes of terrestrial organic matter towards the recording site. For example, organic matter may be supplied directly through surface run-off from surrounding slopes during lake-level highstands or be trapped in low-lying wetlands during lake-level lowstands, depending on basin morphology and lake morphometry. Finally, land-use change fundamentally alters the biome in the catchment of an environmental archive with regard to organic matter sources and fluxes. Land clearance for farming may replace the natural vegetation entirely and modify the soil pool. Slash-and-burn clearance produces large amounts of charred material and combustion products while settlements and animal husbandry can lead to the supply of fecal material. Organic geochemistry provides a wide range of biogeochemical tools to identify both natural and anthropogenic alteration of the terrestrial habitats in the catchment of a depositional environmental archive, revealing changes in vegetation, soil stability, fire frequency and farming.

4.1 Molecular indicators for vegetation change

Waxes are major constituents of the protective outer surface layers of land plants, most prominently of the cuticular layer of leaves. Leaf waxes consist of esters of long-chain *n*-fatty acids and *n*-alcohols as well as *n*-alkanes and ketones, aldehydes, i.e. alkyl lipids (Eglinton and Hamilton 1967). The *n*-fatty acids and *n*-alcohols of leaf waxes predominantly are even-numbered carbon chains in the range of 24 to 38 carbon atoms while *n*-alkanes are dominated by odd-numbered carbon chains of 23-37 carbon atoms. Notably, the length of the alkyl lipid carbon chains preferentially biosynthesized by plants differs between plant species. For example, the dominant *n*-alkane in leaf wax of the common beech (*Fagus sylvatica*) is the C_{27} *n*-alkane while it is the C_{29} *n*-alkane in oak (*Quercus*) and the C_{31} *n*-alkane in grass species growing at the same location (Holtvoeth et al. 2016, Fig. 10).

Fig. 10: Comparison of chain-length distributions of n-fatty acids and n-alkanes in oak and beech leaf litter and in grasses with those of the underlying topsoils and of sediment from the Lake Ohrid Basin, Albania/North Macedonia (modified from Holtvoeth et al. 2016). The intramountainous basin features a high altitude gradient and steep slopes, with the lower altitudes being dominated by oaks and shrubs and the higher altitudes by beech forests

with patchy grassy undergrowth. Note the maximum amount of the C_{31} n-alkane in the topsoil from the beech forest, which results from higher concentrations of n-alkanes in grasses compared to beech leaves and the fact that decaying grass is more likely to being directly incorporated into the topsoil whereas the leaves are mobile, altogether leading to an over-representation of the grass-derived n-alkane. Also note the generally higher proportions of C_{22} and C_{24} n-fatty acid in the topsoils compared to the leaf wax-derived C_{26} to C_{32} n-fatty acids in the leaf litter and grass samples. These compounds are assumed to derive from suberin, a protective bio-polyester found mainly in root tissue, hence, representing belowground biomass. The sediment shown here represents the dry period of the 8.2 ka event that led to vegetation recession and destabilization of soils. The higher than normal amounts of the suberin-derived C_{22} and C_{24} n-fatty acids reflect the increased soil erosion rates during this event.

Considering the vast number of plant species and the narrow range of dominant chain lengths typically biosynthesized, it is highly unlikely that average alkyl lipid chain-length distributions can be assigned to a specific endmember type of vegetation within the catchment of an environmental archive unless biodiversity is extremely low, i.e. dominated by single species. However, shifts in the predominant carbon chain lengths of alkyl lipids observed in a depositional archive will nevertheless be indicative of vegetation changes or changes in organic matter fluxes within the catchment and can be plotted as variability of the average chain length (ACL):

$$ACL = \Sigma(C_n \times n)/\Sigma(C_n) \qquad (10)$$

n-Alkanes have become the prime targets in biomarker-based palaeoenvironmental investigations as they do not contain functional groups, which increases their preservation potential in depositional archives relative to *n*-fatty acids and *n*-alcohols and minimizes lipid extract preparation for analysis (no derivatization of functional groups). The ratio of supposedly grass-derived C_{31} and C_{33} *n*-alkanes over C_{27} and C_{29} *n*-alkanes assumed to dominate leaf waxes of trees is frequently used as indicator of shifts from forests to more open, grassy vegetation and vice-versa. Although not statistically sound on a globally applicable level (Bush and McInerney 2013), this approach appears suitable for vegetation reconstructions on regional scale, in particular, if the dominant species involved can be narrowed down and biogeochemical fingerprinting of the main

leaf wax sources, i.e. vegetation and soils, provides a local modern analogue calibration (e.g. Schwark et al. 2002; Bliedtner et al. 2018). In contrast to the non-specific long-chain (≥25) *n*-alkanes, the mid-chain C_{23} *n*-alkane is a rather reliable biomarker for *Sphagnum* peat mosses (Bush and McInerney 2013). Another more specific alkyl lipid biomarker is the branched C_{29} alcohol nonacosan-10-ol, a prominent compound in leaf waxes of conifers (Matas et al. 2003).

In tropical and subtropical settings, compound-specific stable isotope analysis (CSIA) of leaf-wax derived alkyl lipids can indicate changes in the openness of the vegetation and the relative proportions of trees and grasses. Tropical grasses are typically C_4 plants, named after the first photosynthetic metabolic product consisting of four carbon atoms, while most other higher land plants are C_3 plants. Notably, C_4 plants incorporate significantly higher proportions of the heavy carbon isotope (^{13}C) into their biomass than C_3 plants that strongly discriminate against ^{13}C (O'Leary 1981). As a result, the $^{13}C/^{12}C$ stable carbon isotope ratio of C_4 grass-derived leaf wax compounds distinctly differs from those of C_3 plants such as tropical trees and is expressed as the $\delta^{13}C$ value of a compound relative to a standard:

$$\delta^{13}C = \left(\frac{(^{13}_{0}C/^{12}_{0}C)_{sample}}{(^{13}_{0}C/^{12}_{0}C)_{standard}} - 1\right) * 1000‰ \quad (11)$$

Compound-specific $\delta^{13}C$ values have been successfully applied in numerous palaeoenvironmental studies in tropical settings to reconstruct shifts of C_3 and C_4 vegetation zones (e.g. Huang et al. 2001; Tierney et al. 2010; Sinninghe Damsté et al. 2011). Although *n*-alkanes are preferentially analysed for ease of sample treatment, *n*-fatty acids and *n*-alcohols can also be targeted, particularly in recent/Quaternary sediments where they are often present in significantly higher abundance than *n*-alkanes (Hughen et al. 2004; Russell et al. 2009).

Fig. 11: ***A:*** *Histograms of stable carbon isotope distributions of C3 and C4 plant biomass (from Tipple and Pagani 2007 using data by Cerling and Harris (1999) and* ***B:*** *Reconstruction of the decrease in C4 grass-dominated vegetation in the catchment of Lake Challa (E Africa) since the Last Glacial using compound-specific stable carbon isotope values of the C_{31} n-alkane in the lake sediments (modified from Sinninghe Damste et al.*

2011). Note that maize is a C4 plant and its introduction as agricultural produce outside the tropics can be reconstructed through an equivalent approach.

In analogy to wax-derived alkyl lipids, vegetation changes can also be seen in changing relative amounts of terpenoids that derive from resin, bark and leaf tissue of higher plants (Langenheim 1994). Deciduous trees (angiosperms) produce pentacyclic triterpenoids while conifers (gymnosperms) produce tricyclic diterpenoids (Otto and Simpson 2005; Diefendorf et al. 2012; Giri et al. 2015). Changing ratios of di- and triterpenoids have therefore been used as palaeovegetation proxies (Bechtel et al. 2003; Schouten et al. 2007). Both the fact that deciduous trees and conifers produce substantially different amounts of terpenoids relative to their total biomass and the different preservation potential of di- and triterpenoids introduce significant uncertainty in terpenoid-based reconstructions of the vegetation, with a likely bias towards conifers (Giri et al. 2015). Still, the variability of di- and triterpenoid ratios supports other proxy data sensitive to vegetation change from organic geochemical or palynological analyses. In recent sediments, changing proportions of the triterpenoids α- and β-amyrin also indicate changes in the sources of terrigenous plant matter (Chávez-Lara et al. 2018), with α-amyrin occurring in higher amounts in plant resins and resinous tissue of common subtropical dry forest species *Bursera* and *Protium*, for example (Hernández-Vázquez et al. 2012).

Lignin phenols, finally, provide another established biomarker-based tool to detect vegetation changes. Lignin, after cellulose the second-most abundant structural macromolecule in higher land plant tissue, contains a range of phenolic alcohols of the syringyl, cinnamyl and vanillyl group. Crucially, these phenols are incorporated into lignin in distinctly different proportions, depending on tissue type (woody *vs*. non-woody) and the taxonomic group of vascular plants (angiosperms *vs*. gymnosperms). Ratios of syringyl over vanillyl (S/V) and cinnamyl over vanillyl alcohol (C/V) can therefore be used to reconstruct, for example, changes in the supply of plant matter from conifers (gymnopsperms) or grasslands within the catchment of a depositional archive (Hedges and Mann 1979; Fuhrmann et al. 2003; Hyodo et al. 2017) or to trace the spatial distribution of terrestrial organic matter in marine sediments (Smith et al. 2012; Seki et al. 2014).

4.2 Molecular indicators for the supply of soil organic matter

To date, there is no single geochemical proxy to reliably quantify the amount of soil organic matter buried in a sedimentary record. This is due to the large molecular overlap between plant litter and soil organic matter, resulting from a continuum of degradation stages. Very few biomarkers have been found that exclusively represent belowground plant biomass, i.e. root material, one of them being α,ω-alkanedioic acids, or diacids, that derive from the protective polyester suberin in root tissue (Mendez-Millan et al. 2011; Ji et al. 2015). Suberin consists of alternating layers of aromatic and aliphatic compounds (*n*-fatty acids, *n*-alcohols, ω-hydroxy acids, α,ω-diacids), with characteristic chains of 22 or 24 carbon atoms in the aliphatic layer (Molina et al. 2006; Graca and Santos 2007). The C_{22} and C_{24} ω-hydroxy acids are major compounds of suberin but can also derive from other tissue types, leaving the mid-chain diacids as the only reliable indicators for root material supply. While root-derived lipids are not quantitatively representative for belowground biomass or soil organic matter buried in a sediment, variable proportions of C_{22} and C_{24} alkyl lipids relative to long-chain (> C_{24}) leaf wax-derived compounds indicate changes in the terrestrial carbon pool dynamics (Holtvoeth et al. 2016; Holtvoeth et al. 2017). Compound-specific radiocarbon analysis (CSRA) of alkyl lipids can also reveal changes in the supply of pre-aged, i.e. soil-derived material through age offsets with the sediment age (Smittenberg et al. 2006; Gierga et al. 2016). Since each alkyl lipid fraction represents a mixture of fresh and fossil compounds this approach needs to be combined with other proxies sensitive to soil supply in order to assess the relative amount of fossil compounds, thus, enabling an estimation of terrestrial residence time.

Biomarkers from strains of soil bacteria provide an alternative to root-derived compounds for reconstructing the variable input of soil organic matter towards a depositional archive. A series of branched glycerol-dibiphanyl-glycerol tetraethers (brGDGTs) are cell membrane lipids of anaerobic bacteria in soils. A number of structurally related isoprenoidal GDGTs (iGDGTs), on the other hand, is exclusively produced by aquatic Thaumarchaeota. The ratio of specific branched and isoprenoidal GDGTs, the so-called BIT index, was therefore defined to reflect the changing proportions of soil organic matter supply as represented by the bacterial lipids relative to aquatic production (Hopmans et al. 2004; Weijers et al. 2006). The BIT index has been applied successfully in reconstructions of environmental change on a range of time

scales (Cao et al. 2017; Mayser et al. 2017) and studies tracking the dispersal of terrestrial organic matter in the marine realm using marine surface sediments off major point sources, i.e. rivers with large terrestrial catchments (Smith et al. 2012; Seki et al. 2014). The approach assumes that brGDGTs are representative of soil organic matter and that iGDGT production in the waterbody does not vary to the same extent as soil organic matter supply. It appears, however, that Thaumarchaeota thrive in low-nutrient settings (Konneke et al. 2014), i.e. iGDGT production may be lower under eutrophic conditions and bias the BIT index towards seemingly increased soil organic matter input. In depositional settings with persistently high terrestrial input such as smaller lake basins, BIT value variability may thus be driven by iGDGT production under variable nutrient levels (Smith et al. 2012), allowing for an alternative interpretation of the BIT index as proxy for a changing nutrient regime (Panagiotopoulos et al. 2020). Some brGDGTs have been found to also be produced in the marine water column (Zell et al. 2015) and in lake water (Weber et al. 2015), requiring a local calibration or complementary proxy data.

4.3 Bulk organic matter characteristics indicating soil organic matter supply

During microbial breakdown, soil organic matter typically becomes enriched in ^{13}C relative to ^{12}C and in total nitrogen (N_{tot}) relative to organic carbon (C_{org}) to various degrees, i.e. bulk $\delta^{13}C_{org}$ values of soil organic matter increase while C_{org}/N_{tot} ratios decrease. Both bulk $\delta^{13}C_{org}$ values and C_{org}/N_{tot} ratios have been popular as fast and low-cost proxies to assess the relative proportions of aquatic and terrigenous organic matter in sediments, typically using two end-member values for aquatic and terrestrial plant biomass. However, due to the diagenetic continuum from plant litter to heavily degraded soil organic matter a single terrestrial end-member does not exist. In fact, degradation of terrigenous organic matter in soils can produce a terrestrial sedimentary organic matter fraction with bulk $\delta^{13}C_{org}$ values and C_{org}/N_{tot} ratios similar to those characterizing organic matter from aquatic sources, leading to severe underestimation of terrestrial organic matter burial and erroneous carbon budgets (Holtvoeth et al. 2005). Nevertheless, as bulk $\delta^{13}C_{org}$ values and C_{org}/N_{tot} ratios of sediments with high allochthonous organic matter input can also be determined by changes in terrestrial organic matter quality rather than quantity, these proxies can help identifying phases of enhanced soil erosion and associated soil organic matter supply, in particular, if bulk data of potential soil sources is available. In metal-rich soils such as tropical and

subtropical lateritic soils, organic compounds can be bound firmly to the clay fraction through coupling to the metal oxyhydroxides that cover the clay mineral surfaces. Such stabilized organic matter can be detected by Rock-Eval pyrolysis as it is broken up into volatile compounds at significantly higher temperature compared to non-bound soil organic matter (Holtvoeth et al. 2005).

5. Climate forcing versus land-use change

Untangling climate versus anthropogenic induced landscape change is often challenging. This holds particularly true when climate change temporally coincides with the first arrival of humans at a study site and/or technological advancements in the society. The first step to untangle these two potential causes of landscape change is to reliably establish a record of regional climate change and anthropogenic occupation. This can be obtained for example by means of traditional palaeo-climate proxy analyses on a palaeoclimate archive, and by means of archeological and/or historical research. Human presence in a given catchment can also be confirmed by the occurrence of cultivated pollen taxa in a depositional archive. In the Mediterranean realm, for example, the occurrence of taxa such as *Juglans* (walnut), *Olea* (olive), *Castanea* (chestnut) and *Cerealia* (group of herbaceous taxa indicating the presence of fields) are used as widespread indicators of increasing human activity (Mercuri et al. 2013; Panagiotopoulos et al. 2013; Masi et al. 2018). Distinction of natural and anthropogenic causes of landscape change, as inferred from previously discussed geochemical methods, is then often based on the pure absence or presence of climate change, first human occupation, or technical advancements in the society (e.g. Rothacker et al. 2018). In some cases, the occurrence of distinct depositional features, such as colluvium deposits in central Europe (cf. section 2), are interpreted as stand-alone indicators of human land use and the erosion of bare soils (Dotterweich 2013). Land-use change for settlement and agricultural purposes is often associated with the initial clearance of the pre-existing (natural) vegetation and more or less substantial earthworks, from simple field clearance or construction of a drainage system to terracing slopes, leading to at least temporary soil destabilization and erosion. Both vegetation change and soil erosion can be recognised as such in depositional environmental archives through the application of geochemical approaches described above.

In addition, there are biogeochemical tools that identify human activity as the main driver of observed environmental change, beyond timing and rate of change. Land

clearance is frequently associated with burning of the original vegetation, as are agricultural practices such as stubble burning. This can be seen in depositional archives as increasing amounts of charred particulate material (charcoal, black carbon) as well as molecular combustion products such as monosaccharide anhydrides (MAs) and polycyclic aromatic hydrocarbons (PAHs). The latter are produced from incomplete combustion of organic matter while the former derive from the combustion of cellulose and hemicellulose (Simoneit 2002). While PAHs and MAs are also a product of natural wild fires, an increase in the amount of PAHs beyond the natural background level likely indicates human activity (e.g. D'Anjou et al. 2012).

Some crops biosynthesize species-specific biomarkers or have a distinct isotope fingerprint and that confirms their cultivation in a catchment if observed in sediments. Gramineae produce a range of pentacyclic triterpenoids (Jacob et al. 2005) of which miliacin has been successfully used as indicator for the cultivation of millet in a lacustrine catchment (Jacob et al. 2008). A more recent major crop in many parts of the world outside the Americas is maize, which is a C_4 grass and thus produces ^{13}C-enriched compounds that can be used to reconstruct its introduction in agricultural production (Tankersley et al. 2019). Human settlement and animal husbandry also produce large amounts of fecal material that is easily mobilized and exported towards a depositional archive. The presence of fecal material is revealed by the sterols coprostanol (5β-cholestan-3β-ol) and epicoprostanol (5β-cholestan-3α-ol) that are formed from cholesterol in the intestines of higher mammals, including humans. In human feces, coprostanol is the main sterol while epicoprostanol is absent (Leeming et al. 1994). Concentrations of both compounds relative to other sterols can therefore be used as indicators for manure or sewage contamination in soils and sediments (Sherwin et al. 1993; Bull et al. 2002; Cordeiro et al. 2008) and also, therefore, in palaeodemography to indicate the establishment of larger human settlements or changes in farming practices (D'Anjou et al. 2012; White et al. 2018).

6. Outlook

Research on Quaternary landscape evolution is a necessity in securing soils as one of our most important resources in the light of increasing pressure by rapid climate change and land use, (section 1). Applying the reviewed methods in palaeo-records allows for the identification and understanding of feedbacks and links between climate forcing, vegetation development, and land use. The geochemical methods are typically applied to

archives recording millennial to multi-millennial timescales (Table 1), with the exception of the geochemical analysis of varved lake sediment records (sections 2, 3.1). However, the timescale of socio-economically relevance to securing soil resources is decades or centuries. Implementing findings of Quaternary landscape evolution into policies based on micro- to macro-scale soil erosion modelling (e.g. Panagos and Katsoyiannis 2019) or global-scale land use change projections (e.g. Ostberg et al. 2018) remains a challenge. Quantifying the boundaries of (bio-)geochemical and physical processes in the Critical Zone's evolution on geological time scales, in particular at times where tipping points in the landscape's evolution are crossed, can improve the precision of modelling attempts on time scales of socio-economically relevance (section 6.1 and 6.2).

6.1 Future directions

Terrestrial land cover change is an essential part of the climate system: it affects the albedo (vegetation cover), terrestrial biogeochemical and geochemical cycles, and marine fertilisation by nutrient supply. Earth system models (ESM) and general circulation models (GCM) implement vegetation and "land-use harmonization" (LUH) models to account for feedbacks between the climate system and the landscape (Ma et al. 2019). LUHs are thereby based on landscape models such as HYDE (Klein Goldewijk et al. 2017) or KK^{10} (Kaplan et al. 2009), predicting anthropogenic land cover change over time. These models are based on population history estimates, population density, and gridded datasets of land suitability for agriculture and pasture (Kaplan et al. 2009; Klein Goldewijk et al. 2017) and therefore inherently contain large uncertainties (Li et al. 2020). Other approaches in modelling land-cover change on geological timescales focus on pollen-based reconstructions inferred from palynological archives such as peats and/or lake sediments. These models estimate vegetation compositions in the geological past at local catchment to regional/continental scale (e.g. Europe, temperate China), and are based on pollen reconstructions from individual depositional archives (Local Vegetation Estimates, LOVE) and multiple records with large catchments (Regional Estimates of Vegetation Abundance, REVEALS, Sugita 2007a, b; Trondman et al. 2015; Li et al. 2020). None of the aforementioned models, however, directly implements quantitative estimates of erosion, silicate weathering, and soil-biosphere evolution, i.e. processes that have a major control on landscape evolution, vegetation development and atmospheric CO_2 drawdown and, thus, on the climate system.

Quantitative models of Quaternary landscape evolution coupling forcing, feedbacks, and interaction between climate, vegetation, land use and the Critical Zone are therefore needed to improve ESMs and GCMs that focus on decadal to centennial time scales. Such models need to be evaluated against quantitative proxy-based reconstructions of landscape change. Being capable of feeding such models with quantitative Quaternary landscape data can help to improve the accuracy of local to global scale management plans.

Developing model-proxy comparisons is of particular importance for major terrestrial carbon sinks such as tropical forests and permafrost soils (Lewis et al. 2009; Koven et al. 2011). Anthropogenic or natural deforestation in the tropics reduces their capacity as a carbon sink while accelerated erosion mobilises old carbon and prevents the recovery of tropical forests as carbon sink (Drake et al. 2019). Thawing of permafrost soils in response to climate warming could accelerate topsoil erosion and thus the amount of greenhouse gases released into the atmosphere from polar regions, which is already taking place today (Koven et al. 2011). More quantitative data in space and time about landscape evolution in these key areas can help to better understand processes related to tipping points in the climate system (Lenton et al. 2019). Implementing information inferred from methods reviewed herein could thus help improve catchment-, regional-, and global-scale management plans to mitigate the impact of environmental change on decadal to centennial time scales.

6.2 Requirements to achieve future directions

The ultimate goal of developing and improving quantitative models describing the Critical Zone's evolution on geological time scales still requires significant progress in our capability to quantify biogeochemical, physical, and chemical processes in the Earth's surface. Advancements in more sophisticated geochemical analytical methods, further developments of existing methods, more inter-comparisons between the different methods (interdisciplinary approaches), and accessible data storage of quantitative Quaternary landscape change through space and time are all required, as outlined in more detail below.

More analytical techniques to better infer palaeo-erosion rates that are independent of the amount of material deposited are still required to improve our capability to quantify landscape evolution at a given time in the geological past. Erosion rates inferred from the amount of detrital matter being deposited (e.g. in colluvial deposits or a lake basin)

are biased since not all mobilised material is stored in the analysed archive. Most promising methods for estimating palaeo-erosion rates are in-situ cosmogenic nuclides and U isotopes. U isotopes benefit from its applicability to fine-grained sedimentary archives, which form most continuous, highly resolved palaeoenvironmental archives. Such archives can also be used to study past weathering intensities (radiogenic isotopes) and terrestrial habitat change (organic geochemistry) simultaneously. Ideally, geochemical data is also combined with biogenic proxies (pollen) and archaeological data to reconstruct the separate evolution of past climate, vegetation, soil erosion, weathering and their relationships to human activities over the last few millennia (Bayon et al. 2019).

Databases such as for example OCTOPUS for cosmogenic nuclide-derived denudation rates (Codilean et al. 2018) need to be extended to store different types of data provided by the geochemical methods reviewed herein. Expansion of such databases will require larger datasets, both in terms of sample count and the number of methods applied, and a database structure that provides fast and easy navigation through space and time. Combining the information obtained from different archives and methods also requires precise chronological alignments, which are particularly difficult to obtain in non-continuous sedimentary environments.

If data from different geochemical methods are increasingly combined there is also a need for the development of more sophisticated numerical models to analyse large sets of quantitative data. Challenges might also arise in the combination of different methods. For instance, cosmogenic nuclides and uranium isotopes provide quantitative estimates about catchment erosion, but the numerical output is provided in loss of soil thickness per year (usually in mm/yr) for cosmogenic nuclides, and as catchment residence time (usually in kyr, i.e. time between comminution and final deposition) for uranium isotopes. This task becomes even more complex when quantitative data (e.g. for catchment erosion) is compared to more semi-quantitative and qualitative data (e.g. biogeochemical cycles, terrestrial habitat change, or weathering intensities) across different sites.

7. Conclusions

An extensive portfolio of organic and inorganic geochemical methods have become available to study the three main elements controlling the Critical Zone's evolution over time: (a) silicate weathering and the in-situ formation of regolith (using elemental

ratios, Sr, Hf, inorganic C isotopes), (b) erosion and transport (sediment accumulation, cosmogenic nuclides, U isotopes, elemental ratios), and (c) terrestrial habitats and biogeochemical cycles (organic geochemistry). Some methods are now routinely applied in Quaternary landscape research (such as for example cosmogenic nuclides, element geochemistry and organic geochemistry), while other relatively new methods show increasing evidence about their potential (e.g. metal stable and radiogenic isotopes). Developing and implementing new methods (such as U isotope as quantitative measure for catchment erosion) is in particular necessary to improve our capabilities in inferring more quantitative estimates about Quaternary landscape change.

There is a strong need for further multiproxy and multidisciplinary studies combining the methods in sedimentary archives reviewed. For instance, organic geochemical methods (providing insights soil organic matter mobilization, BIT index) compared with methods used for the reconstruction of weathering and erosion (e.g. element geochemistry, metal and radiogenic isotopes) can provide a comprehensive picture about Critical Zone's evolution over time. Such research has a high potential to provide better insights on internal feedback mechanisms between weathering, erosion, and terrestrial habitat change that can amplify or mitigate the Critical Zone's response to climate forcing and land use. Such findings would also have a high significance to improving Earth System and General Circulation Models, since terrestrial-atmospheric interactions are an essential part of our climate system.

Table 1: Key literature for each reviewed geochemical method. This list encompasses journal articles introducing new methods and comprehensive reviews.

Reference	Reference Type	Significance	
Dreibrodt et al. (2010)	Review	Review about the potential and limitations using geochronolgical and classical sedimentary information from continuous and discontinuous archives displayed in Fig. 1.	Sediment Chronology and sediment accumulation (Section 2)
(Dotterweich 2008, 2013)	Reviews	European (2008) and global (2013) synthesis on catchment erosion: Methods and major findings	
Croudace et	Journal	Descriptions, evaluations, and introduction of XRF-core scanning	i s t

al. (2006)	Article	technologies	
Davies et al. (2015)	Book Chapter	In-depth review of literature using XRF-core scanning elements and elemental ratio on lacustrine sediments for reconstruction of catchment erosion	
Arnaud et al. (2016)	Review	Review focusing on methodological approaches to reconstruct erosion using XRF core scanning technologies with a particular focus on flood dynamics. Regional focus on the European Alps.	
(Croudace et al. 2019a, b)	Journal Articles	State of the art and future perspectives of X-ray core scanner technologies. Both manuscripts are part of a special issue "Advances in Data Quantification and Application of high resolution XRF Core Scanners"	
Leng and Barker (2006)	Book	Comprehensive introduction to the application of stable (carbon) isotopes in palaeoenvironmental research for lacustrine, marine, and speleothem archives.	**Bulk inorganic carbon isotopes (Section 3.2)**
Leng and Marshall (2004)	Review	Comprehensive review on the application of stable, non-metal isotope analyses as palaeoclimate and –environmental proxy.	
DePaolo et al. (2006)	Journal article	Introduction of U isotope analyses as measure for sediment transport time and catchment erosion	**Metal Stable and Radiogenic Isotopes (Section 3.3)**
Dosseto and Schaller (2016)	Review article	Comprehensive review of limitations and potential of uranium and cosmogenic nuclide analyses as measure for catchment erosion	
Banner (2004) and Blum and Erel (2003)	Review articles	These two articles provide generalities on radiogenic isotope systems and on their general behaviour during continental weathering. Various examples are given on their application in the sedimentary record (Banner, 2004) and in hydrological studies (Blum and Erel, 2003).	
Dunai (2010)	Book	Provides a comprehensive and accessible introduction to cosmogenic nuclide analysis. More recent reviews also include Granger et al (2013) and Granger and Riebe (2014). Also relevant, although now outdated, is the EPSL Frontiers paper by von Blanckenburg (2005).	**In-situ cosmogenic nuclide (Section 3.4)**
(Bierman et al. 2002; Niedermann 2002)	Book chapters	Despite their age, both texts are useful to those looking for an introduction to the technique in that they present details on sample preparation and Be and Al chemistry (Bierman et al, 2002), and Ne and He isotope systematics (Niedermann et al 2002).	
Granger (2006)	Book chapter	Comprehensive review of ^{26}Al-^{10}Be burial dating with examples of applications to geology and geomorphology.	
Balco and	Journal article	The first paper to describe an ^{26}Al-^{10}Be isochron method for	

Rovey (2008)		cosmogenic-nuclide dating of buried soils and sediments.	
Hidy et al. (2010)	Journal article	Describes a Monte Carlo approach to modelling exposure ages from depth-profiles of cosmogenic nuclides. Also produced a set of MATLAB scripts for this purpose that have been widely used by the research community.	
Peters et al. (2005)	Book	Detailed introduction of the biomarker concept, explaining the origins of biomarkers, analytical techniques and applications in environmental and archaeological research.	**Organic geochemical proxies (Section 4)**
Freeman and Pancost (2014)	Book/Review	Compact review of biomarker applications for the reconstruction of terrestrial environmental change.	
Holtvoeth et al. (2019)	Review	Comprehensive review of principles and applications of compound-specific isotope analyses (CSIA) for lacustrine sediments.	
Fuhrmann et al. (2003)	Journal article	Example of a multi-method palaeoenvironmental study applying bulk proxies, biomarker analyses, compound-specific isotope analyses and organic petrology.	

Table 2: Applicability of the methods reviewed

Method	**Sediment composition / mineralogy**	**Grain size**	**Applicable time span (ka)**	**Catchment geology**	**Information derived**	**Quantitative / Qualitative***
Sediment chronology	Depending on dating method	Depending on dating method	Depending on dating method	Depending on dating method	Sediment accumulation / erosion	Quantitative / Qualitative
Element geochemistry	Usually siliciclastic sediments	No limitations	No limitations	No limitations	Erosion and weathering	Qualitative
Bulk inorganic carbon isotopes	Authigenic or endogenic carbonates	n/a	No limitations / depending on preservation	No limitations, limestone-rich catchment for application on carbonates	Soil evolution, limestone weathering	Qualitative
U isotopes	siliciclastic sediments	<63µm (silt and clay)	>1 ka < 400 ka	Usually bedrock older 1 Ma	Erosion, sediment residence time (in kyrs)	Quantitative
Hf, Nd, Pb isotopes	siliciclastic sediments, authigenic Fe-oxide minerals	Clay-size sediments	No limitations	No limitations	Weathering, sediment provenance	Qualitative (weathering), quantitative (provenance)
Cosmogenic nuclides	Quartz	>150 µm. Most common for	Limited by half-life of chosen	Quartz bearing lithologies	Erosion rate (in mm/kyr); sediment	Cosmogenic nuclides

		basin wide denudation studies: 250 – 500 µm. depth-profile dating and burial dating studies: pebbles to cobbles	nuclide or nuclide pair; Burial ages from a few ka (^{14}C-^{10}Be pair) to 10 Ma (^{10}Be-^{21}Ne pair)		deposition age (kyr to Myr)	
Organic geochemistry	Organic matter	No limitations	No limitations	No limitations	Terrestrial habitat change, soil organic matter supply	Qualitative

*Highlights if quantitative or qualitative data about landscape evolution (e.g. erosion rates in mm/yr) are provided.

References

Anderson NJ, Bennion H, Lotter AF (2014) Lake eutrophication and its implications for organic carbon sequestration in Europe. Global Change Biology 20 (9):2741-2751. doi:10.1111/gcb.12584

Anderson RS, Repka JL, Dick GS (1996) Explicit treatment of inheritance in dating depositional surfaces using in situ Be-10 and Al-26. Geology 24 (1):47-51. doi:Doi 10.1130/0091-7613(1996)024<0047:Etoiid>2.3.Co;2

Argento DC, Stone JO, Reedy RC, O'Brien K (2015a) Physics-based modeling of cosmogenic nuclides part I - Radiation transport methods and new insights. Quaternary Geochronology 26:25-43. doi:10.1016/j.quageo.2014.09.004

Argento DC, Stone JO, Reedy RC, O'Brien K (2015b) Physics-based modeling of cosmogenic nuclides part II - Key aspects of in-situ cosmogenic nuclide production. Quaternary Geochronology 26:44-55. doi:10.1016/j.quageo.2014.09.005

Arnaud F, Poulenard J, Giguet-Covex C, Wilhelm B, Révillon S, Jenny J-P, Revel M, Enters D, Bajard M, Fouinat L, Doyen E, Simonneau A, Pignol C, Chapron E, Vannière B, Sabatier P (2016) Erosion under climate and human pressures: An alpine lake sediment perspective. Quaternary Science Reviews 152:1-18. doi:10.1016/j.quascirev.2016.09.018

Arnaud F, Révillon S, Debret M, Revel M, Chapron E, Jacob J, Giguet-Covex C, Poulenard J, Magny M (2012) Lake Bourget regional erosion patterns reconstruction reveals Holocene NW European Alps soil evolution and paleohydrology. Quaternary Science Reviews 51:81-92. doi:10.1016/j.quascirev.2012.07.025

Aubert D, Stille P, Probst A (2001) REE fractionation during granite weathering and removal by waters and suspended loads: Sr and Nd isotopic evidence. Geochimica Et Cosmochimica Acta 65 (3):387-406. doi:Doi 10.1016/S0016-7037(00)00546-9

Baartman JEM, Masselink R, Keesstra SD, Temme AJAM (2013) Linking landscape morphological complexity and sediment connectivity. Earth Surface Processes and Landforms 38 (12):1457-1471. doi:10.1002/esp.3434

Balco G, Rovey CW (2008) An Isochron Method for Cosmogenic-Nuclide Dating of Buried Soils and Sediments. Am J Sci 308 (10):1083-1114. doi:10.2475/10.2008.02

Balco G, Shuster DL (2009) Production rate of cosmogenic Ne-21 in quartz estimated from Be-10, Al-26, and Ne-21 concentrations in slowly eroding Antarctic bedrock surfaces. Earth and Planetary Science Letters 281 (1-2):48-58. doi:10.1016/j.epsl.2009.02.006

Balco G, Stone JO, Lifton NA, Dunai TJ (2008) A complete and easily accessible means of calculating surface exposure ages or erosion rates from Be-10 and Al-26 measurements. Quaternary Geochronology 3 (3):174-195. doi:10.1016/j.quageo.2007.12.001

Banner JL (2004) Radiogenic isotopes: systematics and applications to earth surface processes and chemical stratigraphy. Earth-Science Reviews 65 (3-4):141-194. doi:10.1016/S0012-8252(03)00086-2

Bar-Matthews M, Ayalon A (2004) Speleothems as palaeoclimate indicators, a case study from Soreq Cave located in the Eastern Mediterranean Region, Israel. In: Batterbee R, Gasse F, Stickley C (eds) Past climate variability through Europe and Africa. Springer, Dordrecht, pp 363-392

Bayon G, Burton KW, Soulet G, Vigier N, Dennielou B, Etoubleau J, Ponzevera E, German CR, Nesbitt RW (2009) Hf and Nd isotopes in marine sediments: Constraints on global silicate weathering. Earth and Planetary Science Letters 277 (3-4):318-326. doi:10.1016/j.epsl.2008.10.028

Bayon G, Dennielou B, Etoubleau J, Ponzevera E, Toucanne S, Bermell S (2012) Intensifying weathering and land use in Iron age central Africa. Science 335 (6073):1219-1222. doi:10.1126/science.1215400

Bayon G, Schefuss E, Dupont L, Borges AV, Dennielou B, Lambert T, Mollenhauer G, Monin L, Ponzevera E, Skonieczny C, Andre L (2019) The roles of climate and human land-use in the late Holocene rainforest crisis of Central Africa. Earth and Planetary Science Letters 505:30-41. doi:10.1016/j.epsl.2018.10.016

Bayon G, Skonieczny C, Delvigne C, Toucanne S, Bermell S, Ponzevera E, Andre L (2016) Environmental Hf-Nd isotopic decoupling in World river clays. Earth and Planetary Science Letters 438:25-36. doi:10.1016/j.epsl.2016.01.010

Bechtel A, Sachsenhofer RF, Markic M, Gratzer R, Lücke A, Püttmann W (2003) Paleoenvironmental implications from biomarker and stable isotope investigations on the Pliocene Velenje lignite seam (Slovenia). Organic Geochemistry 34 (9):1277-1298. doi:10.1016/s0146-6380(03)00114-1

Berner RA (1994) GEOCARB II: A revised model of atmospheric CO[sub 2] over phanerozoic time. doi:10.2475/ajs.294.1.56

Bierman PR (2004) Rock to sediment - Slope to sea with Be-10 - Rates of landscape change. Annu Rev Earth Pl Sc 32:215-255. doi:10.1146/annurev.earth.32.101802.120539

Bierman PR, Caffee MW, Davis PT, Marsella K, Pavich M, Colgan P, Mickelson D, Larsen J (2002) Rates and timing of earth surface processes from in situ-produced cosmogenic Be-10. Beryllium: Mineralogy, Petrology, and Geochemistry 50:147-205. doi:DOI 10.2138/rmg.2002.50.4

Bierman PR, Steig EJ (1996) Estimating rates of denudation using cosmogenic isotope abundances in sediment. Earth Surface Processes and Landforms 21 (2):125-139. doi:Doi 10.1002/(Sici)1096-9837(199602)21:2<125::Aid-Esp511>3.0.Co;2-8

Blaauw M, Christen JA, Bennett KD, Reimer PJ (2018) Double the dates and go for Bayes — Impacts of model choice, dating density and quality on chronologies. Quaternary Science Reviews 188:58-66. doi:10.1016/j.quascirev.2018.03.032

Bliedtner M, Schafer IK, Zech R, von Suchodoletz H (2018) Leaf wax n-alkanes in modern plants and topsoils from eastern Georgia (Caucasus) - implications for reconstructing regional paleovegetation. Biogeosciences 15 (12):3927-3936. doi:10.5194/bg-15-3927-2018

Blum JD, Erel Y (1995) A Silicate Weathering Mechanism Linking Increases in Marine Sr-87/Sr-86 with Global Glaciation. Nature 373 (6513):415-418. doi:DOI 10.1038/373415a0

Blum JD, Erel Y (2003) Radiogenic Isotopes in Weathering and Hydrology. In: Holland HD, Turekian KK (eds) Treatise on Geochemistry. Pergamon, Oxford, pp 365-392. doi:10.1016/B0-08-043751-6/05082-9

Borchers B, Marrero S, Balco G, Caffee M, Goehring B, Lifton N, Nishiizumi K, Phillips F, Schaefer J, Stone J (2016) Geological calibration of spallation production rates in the CRONUS-Earth project. Quaternary Geochronology 31:188-198. doi:10.1016/j.quageo.2015.01.009

Boyle EA, Edmond JM, Sholkovitz ER (1977) Mechanism of Iron Removal in Estuaries. Geochimica Et Cosmochimica Acta 41 (9):1313-1324. doi:Doi 10.1016/0016-7037(77)90075-8

Boyle JF, Chiverrell RC, Schillereff D (2015) Approaches to Water Content Correction and Calibration for µXRF Core Scanning: Comparing X-ray Scattering with Simple Regression of Elemental Concentrations. In: Croudace IW, Rothwell RG (eds) Micro-XRF Studies of Sediment Cores. Applications of a non-destructive tool for the environmental sciences. Springer Netherlands, Dordrecht, pp 373-390. doi:10.1007/978-94-017-9849-5_14

Brown ET (2011) Lake Malawi's response to "megadrought" terminations: Sedimentary records of flooding, weathering and erosion. Palaeogeography, Palaeoclimatology, Palaeoecology 303 (1-4):120-125. doi:10.1016/j.palaeo.2010.01.038

Brown ET, Stallard RF, Larsen MC, Raisbeck GM, Yiou F (1995) Denudation Rates Determined from the Accumulation of in Situ-Produced Be-10 in the Luquillo Experimental Forest, Puerto-Rico. Earth and Planetary Science Letters 129 (1-4):193-202. doi:Doi 10.1016/0012-821x(94)00249-X

Bull ID, Lockheart MJ, Elhmmali MM, Roberts DJ, Evershed RP (2002) The origin of faeces by means of biomarker detection. Environment International 27 (8):647-654. doi:10.1016/S0160-4120(01)00124-6

Bush RT, McInerney FA (2013) Leaf wax n-alkane distributions in and across modern plants: Implications for paleoecology and chemotaxonomy. Geochimica et Cosmochimica Acta 117:161-179. doi:10.1016/j.gca.2013.04.016

Cao Y, Xing L, Zhang T, Liao WH (2017) Multi-proxy evidence for decreased terrestrial contribution to sedimentary organic matter in coastal areas of the East China Sea during the past 100years. Sci Total Environ 599-600:1895-1902. doi:10.1016/j.scitotenv.2017.05.159

Carretier S, Regard V, Leanni L, Farias M (2019) Long-term dispersion of river gravel in a canyon in the Atacama Desert, Central Andes, deduced from their Be-10 concentrations. Scientific Reports 9. doi:10.1038/s41598-019-53806-x

Cazes G, Fink D, Codilean AT, Fülöp R-H, Fujioka T, Wilcken KM (2020) 26Al/10Be ratios reveal the source of river sediments in the Kimberley, NW Australia. Earth Surface Processes and Landforms 45 (2):424-439. doi:10.1002/esp.4744

Chatterjee A, Ray JS (2017) Sources and depositional pathways of mid-Holocene sediments in the Great Rann of Kachchh, India: Implications for fluvial scenario during the Harappan Culture. Quaternary International 443:177-187. doi:10.1016/j.quaint.2017.06.008

Chávez-Lara CM, Holtvoeth J, Roy PD, Pancost RD (2018) A 27cal ka biomarker-based record of ecosystem changes from lacustrine sediments of the Chihuahua Desert of Mexico. Quaternary Science Reviews 191:132-143. doi:10.1016/j.quascirev.2018.05.013

Chmeleff J, von Blanckenburg F, Kossert K, Jakob D (2010) Determination of the Be-10 half-life by multicollector ICP-MS and liquid scintillation counting. Nucl Instrum Meth B 268 (2):192-199. doi:10.1016/j.nimb.2009.09.012

Codilean AT (2006) Calculation of the cosmogenic nuclide production topographic shielding scaling factor for large areas using DEMs. Earth Surface Processes and Landforms 31 (6):785-794. doi:10.1002/esp.1336

Codilean AT, Bishop P, Stuart FM, Hoey TB, Fabel D, Freeman SPHT (2008) Single-grain cosmogenic 21Ne concentrations in fluvial sediments reveal spatially variable erosion rates. Geology 36 (2):159. doi:10.1130/g24360a.1

Codilean AT, Munack H, Cohen TJ, Saktura WM, Gray A, Mudd SM (2018) OCTOPUS: an open cosmogenic isotope and luminescence database. Earth Syst Sci Data 10 (4):2123-2139. doi:10.5194/essd-10-2123-2018

Cogez A, Meynadier L, Allègre C, Limmois D, Herman F, Gaillardet J (2015) Constraints on the role of tectonic and climate on erosion revealed by two time series analysis of marine cores around New Zealand. Earth and Planetary Science Letters 410:174-185. doi:10.1016/j.epsl.2014.11.022

Cordeiro LGSM, Carreira RS, Wagener A LR (2008) Geochemistry of fecal sterols in a contaminated estuary in southeastern Brazil. Organic Geochemistry 39 (8):1097-1103. doi:10.1016/j.orggeochem.2008.02.022

Council NR (2001) Basic Research Opportunities in Earth Science. The National Academies Press, Washington, DC. doi:doi:10.17226/9981

Croudace IW, Löwemark L, Tjallingii R, Zolitschka B (2019a) Current perspectives on the capabilities of high resolution XRF core scanners. Quaternary International 514:5-15. doi:10.1016/j.quaint.2019.04.002

Croudace IW, Löwemark L, Tjallingii R, Zolitschka B (2019b) High resolution XRF core scanners: A key tool for the environmental and palaeoclimate sciences. Quaternary International 514:1-4. doi:10.1016/j.quaint.2019.05.038

Croudace IW, Rindby A, Rothwell RG (2006) ITRAX: description and evaluation of a new multi-function X-ray core scanner. New Techniques in Sediment Core Analysis 267:51-63

Cuven S, Francus P, Lamoureux SF (2010) Estimation of grain size variability with micro X-ray fluorescence in laminated lacustrine sediments, Cape Bounty, Canadian High Arctic. Journal of Paleolimnology 44 (3):803-817. doi:10.1007/s10933-010-9453-1

D'Anjou RM, Bradley RS, Balascio NL, Finkelstein DB (2012) Climate impacts on human settlement and agricultural activities in northern Norway revealed through sediment biogeochemistry. Proceedings of the National Academy of Sciences of the United States of America 109 (50):20332-20337. doi:10.1073/pnas.1212730109

Dannhaus N, Wittmann H, Kram P, Christl M, von Blanckenburg F (2018) Catchment-wide weathering and erosion rates of mafic, ultramafic, and granitic rock from cosmogenic meteoric Be-10/Be-9 ratios. Geochimica Et Cosmochimica Acta 222:618-641. doi:10.1016/j.gca.2017.11.005

Davies SJ, Lamb HF, Roberts JS (2015) Micro-XRF Core Scanning in Paleolimnology: Recent Developments. In: Croudace I, Rothwell RG (eds) Micro-XRF studies of sediment cores, vol 17. Developments in Paleoenvironmental Research. Springer. doi:10.1007/978-94-017-9849-5_7

De Choudens-Sanchez V, Gonzalez LA (2009) Calcite and Aragonite Precipitation Under Controlled Instantaneous Supersaturation: Elucidating the Role of CaCO3 Saturation State and Mg/Ca Ratio on Calcium Carbonate Polymorphism. Journal of Sedimentary Research 79 (6):363-376. doi:10.2110/jsr.2009.043

DePaolo DJ, Lee VE, Christensen JN, Maher K (2012) Uranium comminution ages: Sediment transport and deposition time scales. Comptes Rendus Geoscience 344 (11-12):678-687. doi:10.1016/j.crte.2012.10.014

DePaolo DJ, Maher K, Christensen JN, McManus J (2006) Sediment transport time measured with U-series isotopes: Results from ODP North Atlantic drift site 984. Earth and Planetary Science Letters 248 (1-2):394-410. doi:10.1016/j.epsl.2006.06.004

DiBiase RA (2018) Short communication: Increasing vertical attenuation length of cosmogenic nuclide production on steep slopes negates topographic shielding corrections for catchment erosion rates. Earth Surf Dynam 6 (4):923-931. doi:10.5194/esurf-6-923-2018

Diefendorf AF, Freeman KH, Wing SL (2012) Distribution and carbon isotope patterns of diterpenoids and triterpenoids in modern temperate C-3 trees and their geochemical significance. Geochimica Et Cosmochimica Acta 85:342-356. doi:10.1016/j.gca.2012.02.016

Diefendorf AF, Patterson WP, Holnicer C, Mullins HT (2008) Carbon isotopes of marl and lake sediment organic matter reflect terrestrial landscape change during the late Glacial and early Holocene (16,800 to 5,540 cal yr B.P.): a multiproxy study of lacustrine sediments at Lough Inchiquin, western Ireland. Journal of Paleolimnology 39 (1):101-115. doi:10.1007/s10933-007-9099-9

Dosseto A, Bourdon B, Turner SP (2008) Uranium-series isotopes in river materials: Insights into the timescales of erosion and sediment transport. Earth and Planetary Science Letters 265 (1-2):1-17. doi:10.1016/j.epsl.2007.10.023

Dosseto A, Hesse PP, Maher K, Fryirs K, Turner S (2010) Climatic and vegetation control on sediment dynamics during the last glacial cycle. Geology 38 (5):395-398. doi:10.1130/g30708.1

Dosseto A, Schaller M (2016) The erosion response to Quaternary climate change quantified using uranium isotopes and in situ-produced cosmogenic nuclides. Earth-Science Reviews 155:60-81. doi:10.1016/j.earscirev.2016.01.015

Dotterweich M (2008) The history of soil erosion and fluvial deposits in small catchments of central Europe: Deciphering the long-term interaction between humans and the environment — A review. Geomorphology 101 (1-2):192-208. doi:10.1016/j.geomorph.2008.05.023

Dotterweich M (2013) The history of human-induced soil erosion: Geomorphic legacies, early descriptions and research, and the development of soil conservation—A global synopsis. Geomorphology 201:1-34. doi:10.1016/j.geomorph.2013.07.021

Drake TW, Van Oost K, Barthel M, Bauters M, Hoyt AM, Podgorski DC, Six J, Boeckx P, Trumbore SE, Cizungu Ntaboba L, Spencer RGM (2019) Mobilization of aged and biolabile soil carbon by tropical deforestation. Nature Geoscience 12 (7):541-546. doi:10.1038/s41561-019-0384-9

Dreibrodt S, Lubos C, Terhorst B, Damm B, Bork HR (2010) Historical soil erosion by water in Germany: Scales and archives, chronology, research perspectives. Quaternary International 222 (1-2):80-95. doi:10.1016/j.quaint.2009.06.014

Dunai TJ (2010) Cosmogenic Nuclides - Principles, Concepts and Applications in the Earth Surface Sciences. Cambridge University Press, Cambridge

Dunne J, Elmore D, Muzikar P (1999) Scaling factors for the rates of production of cosmogenic nuclides for geometric shielding and attenuation at depth on sloped surfaces. Geomorphology 27 (1-2):3-11. doi:Doi 10.1016/S0169-555x(98)00086-5

Eglinton G, Hamilton RJ (1967) Leaf Epicuticular Waxes. Science 156 (3780):1322. doi:10.1126/science.156.3780.1322

Erlanger ED, Granger DE, Gibbon RJ (2012) Rock uplift rates in South Africa from isochron burial dating of fluvial and marine terraces. Geology 40 (11):1019-1022. doi:10.1130/G33172.1

Fontanier C, Mamo B, Toucanne S, Bayon G, Schmidt S, Deflandre B, Dennielou B, Jouet G, Garnier E, Sakai S, Lamas RM, Duros P, Tojofuku T, Sale A, Belleney D, Bichon S, Boissier A, Cheron S, Pitel M, Roubi A, Rovere M, Gremare A, Dupre S, Jorry SJ (2018) Are deep-sea ecosystems surrounding Madagascar threatened by land-use or climate change? Deep-Sea Res Pt I 131:93-100. doi:10.1016/j.dsr.2017.11.011

Francke A, Carney S, Wilcox P, Dosseto A (2018) Sample preparation for determination of comminution ages in lacustrine and marine sediments. Chemical Geology 479:123-135. doi:10.1016/j.chemgeo.2018.01.003

Francke A, Dosseto A, Panagiotopoulos K, Leicher N, Lacey JH, Kyrikou S, Wagner B, Zanchetta G, Kouli K, Leng MJ (2019) Sediment residence time reveals Holocene shift from climatic to vegetation control on catchment erosion in the Balkans. Global and Planetary Change 177:186-200. doi:10.1016/j.gloplacha.2019.04.005

Francke A, Wagner B, Just J, Leicher N, Gromig R, Baumgarten H, Vogel H, Lacey JH, Sadori L, Wonik T, Leng MJ, Zanchetta G, Sulpizio R, Giaccio B (2016) Sedimentological processes and environmental variability at Lake Ohrid (Macedonia, Albania) between 637 ka and the present. Biogeosciences 13 (4):1179-1196. doi:10.5194/bg-13-1179-2016

Freeman KH, Pancost RD (2014) Biomarkers for Terrestrial Plants and Climate. In: Holland HD, Turekian KK (eds) Treatise on Geochemistry (Second Edition). Elsevier, Oxford, pp 395-416. doi:10.1016/978-0-08-095975-7.01028-7

Fuhrmann A, Mingram J, Lucke A, Lu HY, Horsfield B, Liu JQ, Negendank JFW, Schleser GH, Wilkes H (2003) Variations in organic matter composition in sediments from Lake Huguang Maar (Huguangyan), South China during the last 68 ka: implications for environmental and climatic change. Organic Geochemistry 34 (11):1497-1515. doi:10.1016/S0146-6380(03)00158-X

Fülöp RH, Codilean AT, Wilcken KM, Cohent TJ, Fink D, Smith AM, Yang B, Levchenko VA, Wacker L, Marx SK, Stromsoe N, Fujioka T, Dunai TJ (in press) Million-year lag times in a post-orogenic sediment conveyor. . Science Advances

Gaillardet J, Dupré B, Louvat P, Allègre CJ (1999) Global silicate weathering and CO2 consumption rates deduced from the chemistry of large rivers. Chemical Geology 159 (1):3-30. doi:10.1016/S0009-2541(99)00031-5

Gierga M, Hajdas I, van Raden UJ, Gilli A, Wacker L, Sturm M, Bernasconi SM, Smittenberg RH (2016) Long-stored soil carbon released by prehistoric land use: Evidence from compound-specific radiocarbon analysis on Soppensee lake sediments. Quaternary Science Reviews 144:123-131. doi:10.1016/j.quascirev.2016.05.011

Giosan L, Ponton C, Usman M, Blusztajn J, Fuller DQ, Galy V, Haghipour N, Johnson JE, McIntyre C, Wacker L, Eglinton TI (2017) Short communication: Massive erosion in monsoonal central India linked to late Holocene land cover degradation. Earth Surf Dynam 5 (4):781-789. doi:10.5194/esurf-5-781-2017

Giri SJ, Diefendorf AF, Lowell TV (2015) Origin and sedimentary fate of plant-derived terpenoids in a small river catchment and implications for terpenoids as quantitative paleovegetation proxies. Organic Geochemistry 82:22-32. doi:10.1016/j.orggeochem.2015.02.002

Goldberg K, Humayun M (2010) The applicability of the Chemical Index of Alteration as a paleoclimatic indicator: An example from the Permian of the Paraná Basin, Brazil. Palaeogeography, Palaeoclimatology, Palaeoecology 293 (1-2):175-183. doi:10.1016/j.palaeo.2010.05.015

Goldstein SJ, Jacobsen SB (1988) Nd and Sr Isotopic Systematics of River Water Suspended Material - Implications for Crustal Evolution. Earth and Planetary Science Letters 87 (3):249-265. doi:Doi 10.1016/0012-821x(88)90013-1

Gontier A, Rihs S, Chabaux F, Lemarchand D, Pelt E, Turpault M-P (2015) Lack of bedrock grain size influence on the soil production rate. Geochimica et Cosmochimica Acta 166:146-164. doi:10.1016/j.gca.2015.06.013

Graca J, Santos S (2007) Suberin: A biopolyester of plants' skin. Macromol Biosci 7 (2):128-135. doi:10.1002/mabi.200600218

Granger DE (2006) A review of burial dating methods using 26Al and 10Be. In: Siame L, Bourlès D, Brown E (eds) In-situ-Produced Cosmogenic Nuclides and Quantification of Geological Processes, vol 415. Geological Society of America Special Paper. Geological Society of America, pp 1-16

Granger DE, Kirchner JW, Finkel R (1996) Spatially averaged long-term erosion rates measured from in situ-produced cosmogenic nuclides in alluvial sediment. J Geol 104 (3):249-257. doi:Doi 10.1086/629823

Granger DE, Muzikar PF (2001) Dating sediment burial with in situ-produced cosmogenic nuclides: theory, techniques, and limitations. Earth and Planetary Science Letters 188 (1-2):269-281. doi:Doi 10.1016/S0012-821x(01)00309-0

Granger DE, Schaller M (2014) Cosmogenic Nuclides and Erosion at the Watershed Scale. Elements 10 (5):369-373. doi:10.2113/gselements.10.5.369

Granger DE, Smith AL (2000) Dating buried sediments using radioactive decay and muogenic production of Al-26 and Be-10. Nucl Instrum Meth B 172:822-826

Gregory BRB, Patterson RT, Reinhardt EG, Galloway JM (2019) The iBox-FC: A new containment vessel for Itrax X-ray fluorescence core-scanning of freeze cores. Quaternary International 514:76-84. doi:10.1016/j.quaint.2018.09.008

Handley HK, Turner S, Afonso JC, Dosseto A, Cohen T (2013a) Sediment residence times constrained by uranium-series isotopes: A critical appraisal of the comminution approach. Geochimica et Cosmochimica Acta 103:245-262. doi:10.1016/j.gca.2012.10.047

Handley HK, Turner SP, Dosseto A, Haberlah D, Afonso JC (2013b) Considerations for U-series dating of sediments: Insights from the Flinders Ranges, South Australia. Chemical Geology 340:40-48. doi:10.1016/j.chemgeo.2012.12.003

Hare VJ, Loftus E, Jeffrey A, Ramsey CB (2018) Atmospheric CO2 effect on stable carbon isotope composition of terrestrial fossil archives. Nature Communications 9 (1):252. doi:10.1038/s41467-017-02691-x

Harel MA, Mudd SM, Attal M (2016) Global analysis of the stream power law parameters based on worldwide Be-10 denudation rates. Geomorphology 268:184-196. doi:10.1016/j.geomorph.2016.05.035

Harlavan Y, Erel Y, Blum JD (1998) Systematic changes in lead isotopic composition with soil age in glacial granitic terrains. Geochimica Et Cosmochimica Acta 62 (1):33-46. doi:Doi 10.1016/S0016-7037(97)00328-1

Harnois L (1988) The CIW index: A new chemical index of weathering. Sedimentary Geology 55 (3):319-322. doi:10.1016/0037-0738(88)90137-6

Hasberg AKM, Bijaksana S, Held P, Just J, Melles M, Morlock MA, Opitz S, Russell JM, Vogel H, Wennrich V, Kwiecien O (2019) Modern sedimentation processes in Lake Towuti, Indonesia, revealed by the composition of surface sediments. Sedimentology 66 (2):675-698. doi:10.1111/sed.12503

Hedges JI, Mann DC (1979) Characterization of Plant-Tissues by Their Lignin Oxidation-Products. Geochimica Et Cosmochimica Acta 43 (11):1803-1807. doi:Doi 10.1016/0016-7037(79)90028-0

Hernández-Vázquez L, Palazon J, Navarro-Ocaña A (2012) The pentacyclic triterpenes α-, β-amyrins: a review of sources and biological activities. In: Rao V (ed) Phytochemicals - A Global Perspective of Their Role in Nutrition and Health, vol 23. IntechOpen Ltd., London, pp 487-502. doi:10.5772/1387

Hidy AJ, Gosse JC, Pederson JL, Mattern JP, Finkel RC (2010) A geologically constrained Monte Carlo approach to modeling exposure ages from profiles of cosmogenic nuclides: An example from Lees Ferry, Arizona. Geochem Geophy Geosy 11. doi:10.1029/2010gc003084

Holtvoeth J, Kolonic S, Wagner T (2005) Soil organic matter as an important contributor to late Quaternary sediments of the tropical West African continental margin. Geochimica Et Cosmochimica Acta 69 (8):2031-2041. doi:10.1016/j.gca.2004.09.030

Holtvoeth J, Rushworth D, Copsey H, Imeri A, Cara M, Vogel H, Wagner T, Wolff GA (2016) Improved end-member characterisation of modern organic matter pools in the Ohrid Basin (Albania, Macedonia) and evaluation of new palaeoenvironmental proxies. Biogeosciences 13 (3):795-816. doi:10.5194/bg-13-795-2016

Holtvoeth J, Vogel H, Valsecchi V, Lindhorst K, Schouten S, Wagner B, Wolff GA (2017) Linear and non-linear responses of vegetation and soils to glacial-interglacial climate change in a Mediterranean refuge. Sci Rep 7 (1):8121. doi:10.1038/s41598-017-08101-y

Holtvoeth J, Whiteside JH, Engels S, Freitas FS, Grice K, Greenwood P, Johnson S, Kendall I, Lengger SK, Lucke A, Mayr C, Naafs BDA, Rohrssen M, Sepulveda J (2019) The paleolimnologist's guide to compound-specific stable isotope analysis - An introduction to principles and applications of CSIA for Quaternary lake sediments. Quaternary Science Reviews 207:101-133. doi:10.1016/j.quascirev.2019.01.001

Hopmans EC, Weijers JWH, Schefuß E, Herfort L, Sinninghe Damsté JS, Schouten S (2004) A novel proxy for terrestrial organic matter in sediments based on branched and isoprenoid tetraether lipids. Earth and Planetary Science Letters 224 (1–2):107-116. doi:10.1016/j.epsl.2004.05.012

Huang Y, Street-Perrott FA, Metcalfe SE, Brenner M, Moreland M, Freeman KH (2001) Climate change as the dominant control on glacial-interglacial variations in C-3 and C-4 plant abundance. Science 293 (5535):1647-1651. doi:DOI 10.1126/science.1060143

Hughen KA, Eglinton TI, Xu L, Makou M (2004) Abrupt tropical vegetation response to rapid climate changes. Science 304 (5679):1955-1959. doi:10.1126/science.1092995

Hyodo F, Kuwae M, Sasaki N, Hayashi R, Makino W, Kusaka S, Tsugeki NK, Ishida S, Ohtsuki H, Omoto K, Urabe J (2017) Variations in lignin-derived phenols in sediments of Japanese lakes over the last century and their relation to watershed vegetation. Organic Geochemistry 103:125-135. doi:10.1016/j.orggeochem.2016.11.001

IPCC (2014) Climate Change 2014: Synthesis Report. Contribution of Working Groups I, II and III to the Fifth Assessment Report of the Intergovernmental Panel on Climate Change. IPCC,

Jacob J, Disnar JR, Arnaud F, Chapron E, Debret M, Lallier-Verges E, Desmet M, Revel-Rolland M (2008) Millet cultivation history in the French Alps as evidenced by a sedimentary molecule. Journal of Archaeological Science 35 (3):814-820. doi:10.1016/j.jas.2007.06.006

Jacob J, Disnar JR, Boussafir M, Albuquerque ALS, Sifeddine A, Turcq B (2005) Pentacyclic triterpene methyl ethers in recent lacustrine sediments (Lagoa do Caco, Brazil). Organic Geochemistry 36 (3):449-461. doi:10.1016/j.orggeochem.2004.09.005

James LA (2013) Impacts of Early Agriculture and Deforestation on Geomorphic Systems. In: Shroder JF (ed) Treatise on Geomorphology. Academic Press, San Diego, pp 48-67. doi:10.1016/B978-0-12-374739-6.00342-0

Ji HS, Ding YJ, Liu XY, Li LQ, Zhang DX, Li ZC, Sun JL, Hashmi MS, Joseph S, Meng YD, Kuzyakov Y, Pan GX (2015) Root-Derived Short-Chain Suberin Diacids from Rice and Rape Seed in a Paddy Soil under Rice Cultivar Treatments. Plos One 10 (5). doi:10.1371/journal.pone.0127474

Jin L, Ogrinc N, Hamilton SK, Szramek K, Kanduc T, Walter LM (2009) Inorganic carbon isotope systematics in soil profiles undergoing silicate and carbonate weathering (Southern Michigan, USA). Chemical Geology 264 (1):139-153. doi:10.1016/j.chemgeo.2009.03.002

Kaplan JO, Krumhardt KM, Zimmermann N (2009) The prehistoric and preindustrial deforestation of Europe. Quaternary Science Reviews 28 (27):3016-3034. doi:10.1016/j.quascirev.2009.09.028

Keeling CD (1979) The Suess effect: 13Carbon-14Carbon interrelations. Environment International 2 (4):229-300. doi:10.1016/0160-4120(79)90005-9

Kigoshi K (1971) Alpha-recoil Thorium-234: Dissolution into water and the uranium-234/uranium-238 disequilibrium in nature. Science 173 (3991):47

Klein Goldewijk K, Beusen A, Doelman J, Stehfest E (2017) Anthropogenic land use estimates for the Holocene – HYDE 3.2. Earth Syst Sci Data 9 (2):927-953. doi:10.5194/essd-9-927-2017

Konneke M, Schubert DM, Brown PC, Hugler M, Standfest S, Schwander T, von Borzyskowski LS, Erb TJ, Stahl DA, Berg IA (2014) Ammonia-oxidizing archaea use the most energy-efficient aerobic pathway for CO2 fixation. Proceedings of the National Academy of Sciences of the United States of America 111 (22):8239-8244. doi:10.1073/pnas.1402028111

Korschinek G, Bergmaier A, Faestermann T, Gerstmann UC, Knie K, Rugel G, Wallner A, Dillmann I, Dollinger G, von Gostomski CL, Kossert K, Maiti M, Poutivtsev M, Remmert A (2010) A new value for the half-life of Be-10 by Heavy-Ion Elastic Recoil Detection and liquid scintillation counting. Nucl Instrum Meth B 268 (2):187-191. doi:10.1016/j.nimb.2009.09.020

Korup O, Densmore AL, Schlunegger F (2010) The role of landslides in mountain range evolution. Geomorphology 120 (1-2):77-90. doi:10.1016/j.geomorph.2009.09.017

Koven CD, Ringeval B, Friedlingstein P, Ciais P, Cadule P, Khvorostyanov D, Krinner G, Tarnocai C (2011) Permafrost carbon-climate feedbacks accelerate global warming. Proc Natl Acad Sci U S A 108 (36):14769-14774. doi:10.1073/pnas.1103910108

Kump LR, Brantley SL, Arthur MA (2000) Chemical Weathering, Atmospheric CO2, and Climate. Annu Rev Earth Pl Sc 28 (1):611-667. doi:10.1146/annurev.earth.28.1.611

Kylander ME, Ampel L, Wohlfarth B, Veres D (2011) High-resolution X-ray fluorescence core scanning analysis of Les Echets (France) sedimentary sequence: new insights from chemical proxies. Journal of Quaternary Science 26 (1):109-117. doi:10.1002/jqs.1438

Lacey JH, Leng MJ, Francke A, Sloane HJ, Milodowski A, Vogel H, Baumgarten H, Zanchetta G, Wagner B (2016) Northern Mediterranean climate since the Middle Pleistocene: a 637 ka stable isotope record from Lake Ohrid (Albania/Macedonia). Biogeosciences 13 (6):1801-1820. doi:10.5194/bg-13-1801-2016

Lacey JH, Leng MJ, Peckover EN, Dean JR, Wilke T, Francke A, Zhang X, Masi A, Wagner B (2018) Investigating the environmental interpretation of oxygen and carbon isotope data from whole and fragmented bivalve shells. Quaternary Science Reviews 194:55-61. doi:10.1016/j.quascirev.2018.06.025

Lal D (1991) Cosmic-Ray Labeling of Erosion Surfaces - Insitu Nuclide Production-Rates and Erosion Models. Earth and Planetary Science Letters 104 (2-4):424-439. doi:Doi 10.1016/0012-821x(91)90220-C

Langenheim JH (1994) Higher-Plant Terpenoids - a Phytocentric Overview of Their Ecological Roles. J Chem Ecol 20 (6):1223-1280. doi:Doi 10.1007/Bf02059809

Lapointe F, Francus P, Lamoureux ST, Saïd M, Cuven S (2012) 1750 years of large rainfall events inferred from particle size at East Lake, Cape Bounty, Melville Island, Canada. Journal of Paleolimnology 48 (1):159-173. doi:10.1007/s10933-012-9611-8

Lee V, DePaolo DJ, Christensen JN (2010a) Uranium-series comminution ages of continental sediments: Case study of a Pleistocene alluvial fan. Earth and Planetary Science Letters 296 (3-4):244-254

Lee VE, DePaolo DJ, Christensen JN (2010b) Uranium-series comminution ages of continental sediments: Case study of a Pleistocene alluvial fan. Earth and Planetary Science Letters 296 (3-4):244-254. doi:10.1016/j.epsl.2010.05.005

Leeming R, Ball A, Ashbolt N, Jones G, Nichols P (1994) Distinguishing between human and animal sources of faecal pollution. Chemistry in Australia 61:434-435

Leng MJ, Barker PA (2006) A review of the oxygen isotope composition of lacustrine diatom silica for palaeoclimate reconstruction. Earth-Science Reviews 75 (1-4):5-27. doi:10.1016/j.earscirev.2005.10.001

Leng MJ, Marshall JD (2004) Palaeoclimate interpretation of stable isotope data from lake sediment archives. Quaternary Science Reviews 23 (7,Äì8):811-831. doi:10.1016/j.quascirev.2003.06.012

Lenton TM, Rockström J, Gaffney O, Rahmstorf S, Richardson K, Steffen W, Schellnhuber HJ (2019) Climate tipping points — too risky to bet against. Nature 575:592-595. doi:10.1038/d41586-019-03595-0

Lewis SL, Lopez-Gonzalez G, Sonké B, Affum-Baffoe K, Baker TR, Ojo LO, Phillips OL, Reitsma JM, White L, Comiskey JA, K M-ND, Ewango CEN, Feldpausch TR, Hamilton AC, Gloor M, Hart T, Hladik A, Lloyd J, Lovett JC, Makana J-R, Malhi Y, Mbago FM, Ndangalasi HJ, Peacock J, Peh KSH, Sheil D, Sunderland T, Swaine MD, Taplin J, Taylor D, Thomas

SC, Votere R, Wöll H (2009) Increasing carbon storage in intact African tropical forests. Nature 457 (7232):1003-1006. doi:10.1038/nature07771

Li F, Gaillard M-J, Cao X, Herzschuh U, Sugita S, Tarasov PE, Wagner M, Xu Q, Ni J, Wang W, Zhao Y, An C, Beusen AHW, Chen F, Feng Z, Goldewijk CGMK, Huang X, Li Y, Li Y, Liu H, Sun A, Yao Y, Zheng Z, Jia X (2020) Towards quantification of Holocene anthropogenic land-cover change in temperate China: A review in the light of pollen-based REVEALS reconstructions of regional plant cover. Earth-Science Reviews 203:103119. doi:10.1016/j.earscirev.2020.103119

Li L, Chen J, Chen T, Chen Y, Hedding DW, Li G, Li L, Li T, Robinson LF, West AJ, Wu W, You C-F, Zhao L, Li G (2018) Weathering dynamics reflected by the response of riverine uranium isotope disequilibrium to changes in denudation rate. Earth and Planetary Science Letters 500:136-144. doi:10.1016/j.epsl.2018.08.008

Li L, Li L, Li G (2017) Uranium comminution age responds to erosion rate semi-quantitatively. Acta Geochimica 39 (3):426-428. doi:10.1007/s11631-017-0182-2

Lifton N, Sato T, Dunai TJ (2014) Scaling in situ cosmogenic nuclide production rates using analytical approximations to atmospheric cosmic-ray fluxes. Earth and Planetary Science Letters 386:149-160. doi:10.1016/j.epsl.2013.10.052

Ma L, Chabaux F, Pelt E, Blaes E, Jin L, Brantley S (2010) Regolith production rates calculated with uranium-series isotopes at Susquehanna/Shale Hills Critical Zone Observatory. Earth and Planetary Science Letters 297 (1-2):211-225. doi:10.1016/j.epsl.2010.06.022

Ma L, Hurtt GC, Chini LP, Sahajpal R, Pongratz J, Frolking S, Stehfest E, Klein Goldewijk K, O' Leary D, Doelman JC (2019) Global Transition Rules for Translating Land-use Change (LUH2) To Land-cover Change for CMIP6 using GLM2. Geosci Model Dev Discuss 2019:1-30. doi:10.5194/gmd-2019-146

Maher K, DePaolo DJ, Christensen JN (2006) U–Sr isotopic speedometer: Fluid flow and chemical weathering rates in aquifers. Geochimica et Cosmochimica Acta 70 (17):4417-4435. doi:10.1016/j.gca.2006.06.1559

Maher K, DePaolo DJ, Lin JCF (2004) Rates of silicate dissolution in deep-sea sediment: in situ measurement using U-234/U-238 of pore fluids. Geochim Cosmochim Acta 68:4629-4648

Makhubela TV, Kramers JD, Scherler D, Wittmann H, Dirks PHGM, Winkler SR (2019) Effects of long soil surface residence times on apparent cosmogenic nuclide denudation rates and burial ages in the Cradle of Humankind, South Africa. Earth Surface Processes and Landforms n/a (n/a). doi:10.1002/esp.4723

Marshall MH, Lamb HF, Huws D, Davies SJ, Bates R, Bloemendal J, Boyle J, Leng MJ, Umer M, Bryant C (2011) Late Pleistocene and Holocene drought events at Lake Tana, the source of the Blue Nile. Global and Planetary Change 78 (3-4):147-161. doi:10.1016/j.gloplacha.2011.06.004

Marston RA (2010) Geomorphology and vegetation on hillslopes: Interactions, dependencies, and feedback loops. Geomorphology 116 (3-4):206-217. doi:10.1016/j.geomorph.2009.09.028

Martin AN, Dosseto A, Kinsley LPJ (2015) Evaluating the removal of non-detrital matter from soils and sediment using uranium isotopes. Chemical Geology 396:124-133. doi:10.1016/j.chemgeo.2014.12.016

Martin AN, Dosseto A, May J-H, Jansen JD, Kinsley LPJ, Chivas AR (2019) Sediment residence times in catchments draining to the Gulf of Carpentaria, northern Australia, inferred

by uranium comminution dating. Geochimica et Cosmochimica Acta 244:264-291. doi:10.1016/j.gca.2018.09.031

Martin-Puertas C, Brauer A, Dulski P, Brademann B (2012) Testing climate–proxy stationarity throughout the Holocene: an example from the varved sediments of Lake Meerfelder Maar (Germany). Quaternary Science Reviews 58:56-65. doi:10.1016/j.quascirev.2012.10.023

Masi A, Francke A, Pepe C, Thienemann M, Wagner B, Sadori L (2018) Vegetation history and paleoclimate at Lake Dojran (FYROM/Greece) during the Late Glacial and Holocene. Climate of the Past 14 (3):351-367. doi:10.5194/cp-14-351-2018

Matas AJ, Sanz MJ, Heredia A (2003) Studies on the structure of the plant wax nonacosan-10-ol, the main component of epicuticular wax conifers. Int J Biol Macromol 33 (1-3):31-35. doi:10.1016/S0141-8130(03)00061-8

Mayser JP, Flecker R, Marzocchi A, Kouwenhoven TJ, Lunt DJ, Pancost RD (2017) Precession driven changes in terrestrial organic matter input to the Eastern Mediterranean leading up to the Messinian Salinity Crisis. Earth and Planetary Science Letters 462:199-211. doi:10.1016/j.epsl.2017.01.029

McPhillips D, Bierman PR, Rood DH (2014) Millennial-scale record of landslides in the Andes consistent with earthquake trigger. Nature Geoscience 7 (12):925-930. doi:10.1038/Ngeo2278

Mendez-Millan M, Dignac MF, Rumpel C, Derenne S (2011) Can cutin and suberin biomarkers be used to trace shoot and root-derived organic matter? A molecular and isotopic approach. Biogeochemistry 106 (1):23-38. doi:10.1007/s10533-010-9407-8

Menozzi D, Dosseto A, Kinsley LPJ (2016) Assessing the effect of sequential extraction on the uranium-series isotopic composition of a basaltic weathering profile. Chemical Geology 446:126-137. doi:10.1016/j.chemgeo.2016.05.031

Mercuri AM, Bandini Mazzanti M, Florenzano A, Montecchi MC, Rattighieri E (2013) Olea, Juglans and Castanea: The CJO group as pollen evidence of the development of human-induced environments in the Italian peninsula. Quaternary International 303:24-42. doi:10.1016/j.quaint.2013.01.005

Molina I, Bonaventure G, Ohlrogge J, Pollard M (2006) The lipid polyester composition of Arabidopsis thaliana and Brassica napus seeds. Phytochemistry 67 (23):2597-2610. doi:10.1016/j.phytochem.2006.09.011

Mook WG, Bommerson JC, Staverman WH (1974) Carbon isotope fractionation between dissolved bicarbonate and gaseous carbon dioxide. Earth and Planetary Science Letters 22 (2):169-176. doi:10.1016/0012-821X(74)90078-8

Moore AK, Granger DE (2019) Calibration of the production rate of cosmogenic Cl-36 from Fe. Quaternary Geochronology 51:87-98. doi:10.1016/j.quageo.2019.02.002

Morlock MA, Vogel H, Nigg V, Ordoñez L, Hasberg AKM, Melles M, Russell JM, Bijaksana S (2018) Climatic and tectonic controls on source-to-sink processes in the tropical, ultramafic catchment of Lake Towuti, Indonesia. Journal of Paleolimnology 61 (3):279-295. doi:10.1007/s10933-018-0059-3

Mudd SM (2017) Detection of transience in eroding landscapes. Earth Surface Processes and Landforms 42 (1):24-41. doi:10.1002/esp.3923

Muzikar P (2008) Cosmogenic nuclide concentrations in episodically eroding surfaces: Theoretical results. Geomorphology 97 (3-4):407-413. doi:10.1016/j.geomorph.2007.08.020

Muzikar P (2009) General models for episodic surface denudation and its measurement by cosmogenic nuclides. Quaternary Geochronology 4 (1):50-55. doi:10.1016/j.quageo.2008.06.004

Muzikar P (2019) Episodic Erosion With a Power Law Probability Density, and the Accumulation of Cosmogenic Nuclides. J Geophys Res-Earth 124 (9):2345-2355. doi:10.1029/2019jf005095

Nesbitt HW, Young GM (1982) Early Proterozoic climates and plate motions inferred from major element chemistry of lutites. Nature 299 (5885):715-717. doi:10.1038/299715a0

Niedermann S (2002) Cosmic-ray-produced noble gases in terrestrial rocks: Dating tools for surface processes. Rev Mineral Geochem 47:731-784. doi:DOI 10.2138/rmg.2002.47.16

O'Leary MH (1981) Carbon isotope fractionation in plants. Phytochemistry 20 (4):553-567. doi:10.1016/0031-9422(81)85134-5

Ostberg S, Boysen LR, Schaphoff S, Lucht W, Gerten D (2018) The biosphere under potential paris outcomes. Earth's Future. doi:10.1002/2017ef000628

Otto A, Simpson MJ (2005) Degradation and preservation of vascular plant-derived biomarkers in grassland and forest soils from Western Canada. Biogeochemistry 74 (3):377-409. doi:10.1007/s10533-004-5834-8

Panagiotopoulos K, Aufgebauer A, Schäbitz F, Wagner B (2013) Vegetation and climate history of the Lake Prespa region since the Late Glacial. Quaternary International 292:157-169. doi:10.1016/j.quaint.2012.05.048

Panagiotopoulos K, Holtvoeth J, Kouli K, Marinova E, Francke A, Cvetkoska A, Jovanovska E, Lacey JH, Lyons ET, Buckel C, Bertini A, Donders T, Just J, Leicher N, Leng MJ, Melles M, Pancost RD, Sadori L, Tauber P, Vogel H, Wagner B, Wilke T (2020) Insights into the evolution of the young Lake Ohrid ecosystem and vegetation succession from a southern European refugium during the Early Pleistocene. Quaternary Science Reviews 227:106044. doi:10.1016/j.quascirev.2019.106044

Panagos P, Katsoyiannis A (2019) Soil erosion modelling: The new challenges as the result of policy developments in Europe. Environmental Research 172:470-474. doi:10.1016/j.envres.2019.02.043

Peters KE, Walters CC, Moldowan JM (2005) The Biomarker Guide - Second Edition, Part I Biomarkers and Isotopes in the Environment and Human History. Cambridge University Press

Portenga EW, Bierman PR (2011) Understanding Earth's eroding surface with 10Be. GSA Today

Post WM, Emanuel WR, Zinke PJ, Stangenberger AG (1982) Soil carbon pools and world life zones. Nature 298 (5870):156-159. doi:10.1038/298156a0

Price JR, Velbel MA (2003) Chemical weathering indices applied to weathering profiles developed on heterogeneous felsic metamorphic parent rocks.

Profe J, Ohlendorf C (2019) X-ray fluorescence scanning of discrete samples – An economical perspective. Quaternary International 514:68-75. doi:10.1016/j.quaint.2018.09.022

Prush VB, Oskin ME (2020) A mechanistic erosion model for cosmogenic nuclide inheritance in single-clast exposure ages. Earth and Planetary Science Letters 536. doi:10.1016/j.epsl.2020.116066

Regattieri E, Zanchetta G, Isola I, Zanella E, Drysdale RN, Hellstrom JC, Zerboni A, Dallai L, Tema E, Lanci L, Costa E, Magri F (2019) Holocene Critical Zone dynamics in an Alpine

catchment inferred from a speleothem multiproxy record: disentangling climate and human influences. Sci Rep 9 (1):17829. doi:10.1038/s41598-019-53583-7

Renberg I, Brannvall ML, Bindler R, Emteryd O (2002) Stable lead isotopes and lake sediments - a useful combination for the study of atmospheric lead pollution history. Science of the Total Environment 292 (1-2):45-54. doi:10.1016/0048-9697(02)00032-3

Repka JL, Anderson RS, Finkel RC (1997) Cosmogenic dating of fluvial terraces, Fremont River, Utah. Earth and Planetary Science Letters 152 (1-4):59-73. doi:Doi 10.1016/S0012-821x(97)00149-0

Romanek CS, Grossman EL, Morse JW (1992) Carbon isotopic fractionation in synthetic aragonite and calcite: Effects of temperature and precipitation rate. Geochimica et Cosmochimica Acta 56 (1):419-430. doi:10.1016/0016-7037(92)90142-6

Rothacker L, Dosseto A, Francke A, Chivas AR, Vigier N, Kotarba-Morley AM, Menozzi D (2018) Impact of climate change and human activity on soil landscapes over the past 12,300 years. Scientific Reports 8 (1). doi:10.1038/s41598-017-18603-4

Russell JM, Mccoy SJ, Verschuren D, Bessems I, Huang Y (2009) Human impacts, climate change, and aquatic ecosystem response during the past 2000 yr at Lake Wandakara, Uganda. Quaternary Research 72 (3):315-324. doi:10.1016/j.yqres.2009.06.008

Schaefer JM, Denton GH, Kaplan MR, Putnam A, Finkel RC, Barrell DJA, Andersen BG, Schwartz R, Mackintosh A, Chinn T, Schluchter C (2009) High-Frequency Holocene Glacier Fluctuations in New Zealand Differ from the Northern Signature. Science 324 (5927):622-625. doi:10.1126/science.1169312

Schillereff DN, Chiverrell RC, Macdonald N, Hooke JM (2014) Flood stratigraphies in lake sediments: A review. Earth-Science Reviews 135:17-37. doi:10.1016/j.earscirev.2014.03.011

Schouten S, Woltering M, Rijpstra WIC, Sluijs A, Brinkhuis H, Damste JSS (2007) The Paleocene-Eocene carbon isotope excursion in higher plant organic matter: Differential fractionation of angiosperms and conifers in the Arctic. Earth and Planetary Science Letters 258 (3-4):581-592. doi:10.1016/j.epsl.2007.04.024

Schwark L, Zink K, Lechterbeck J (2002) Reconstruction of postglacial to early Holocene vegetation history in terrestrial Central Europe via cuticular lipid biomarkers and pollen records from lake sediments. Geology 30 (5):463-466. doi:Doi 10.1130/0091-7613(2002)030<0463:Ropteh>2.0.Co;2

Seki O, Mikami Y, Nagao S, Bendle JA, Nakatsuka T, Kim VI, Shesterkin VP, Makinov AN, Fukushima M, Moossen HM, Schouten S (2014) Lignin phenols and BIT index distributions in the Amur River and the Sea of Okhotsk: Implications for the source and transport of particulate terrestrial organic matter to the ocean. Prog Oceanogr 126:146-154. doi:10.1016/j.pocean.2014.05.003

Sharp Z (2007) Principles of Stable Isotope Geochemistry. Pearson Prentice Hall, New Jersey

Sherwin MR, Vanvleet ES, Fossato VU, Dolci F (1993) Coprostanol (5-Beta-Cholestan-3-Beta-Ol) in Lagoonal Sediments and Mussels of Venice, Italy. Mar Pollut Bull 26 (9):501-507. doi:Doi 10.1016/0025-326x(93)90467-X

Simoneit BRT (2002) Biomass burning - A review of organic tracers for smoke from incomplete combustion. Applied Geochemistry 17 (3):129-162. doi:10.1016/0883-2927(01)0001-0

Sinninghe Damsté J, Verschuren D, Ossebaar J, Blokker J, van Houten R, van der Meer MTJ, Plessen B, Schouten S (2011) A 25,000-year record of climate-induced changes in lowland vegetation of eastern equatorial Africa revealed by the stable carbon-

isotopic composition of fossil plant leaf waxes. Earth and Planetary Science Letters 302 (1-2):236-246. doi:10.1016/j.epsl.2010.12.025

Skov DS, Egholm DL, Jansen JD, Sandiford M, Knudsen MF (2019) Detecting landscape transience with in situ cosmogenic C-14 and Be-10. Quaternary Geochronology 54. doi:10.1016/j.quageo.2019.101008

Small EE, Anderson RS, Repka JL, Finkel R (1997) Erosion rates of alpine bedrock summit surfaces deduced from in situ Be-10 and Al-26. Earth and Planetary Science Letters 150 (3-4):413-425. doi:Doi 10.1016/S0012-821x(97)00092-7

Smith RW, Bianchi TS, Li XX (2012) A re-evaluation of the use of branched GDGTs as terrestrial biomarkers: Implications for the BIT Index. Geochimica Et Cosmochimica Acta 80:14-29. doi:10.1016/j.gca.2011.11.025

Smittenberg RH, Eglinton TI, Schouten S, Damste JSS (2006) Ongoing buildup of refractory organic carbon in boreal soils during the Holocene. Science 314 (5803):1283-1286. doi:10.1126/science.1129376

Struck M, Jansen JD, Fujioka T, Codilean AT, Fink D, Egholm DL, Fulop RH, Wilcken KM, Kotevski S (2018a) Soil production and transport on postorogenic desert hillslopes quantified with Be-10 and Al-26. Geological Society of America Bulletin 130 (5-6):1017-1040. doi:10.1130/B31767.1

Struck M, Jansen JD, Fujioka T, Codilean AT, Fink D, Fulop RH, Wilcken KM, Price DM, Kotevski S, Fifield LK, Chappell J (2018b) Tracking the Be-10-Al-26 source-area signal in sediment-routing systems of arid central Australia. Earth Surf Dynam 6 (2):329-349. doi:10.5194/esurf-6-329-2018

Süfke F, Gutjahr M, Gilli A, Anselmetti FS, Gier L, Eisenhauer A (2019) Early stage weathering systematics of Pb and Nd isotopes derived from a high-Alpine Holocene lake sediment record. Chemical Geology 507:42-53. doi:10.1016/j.chemgeo.2018.12.026

Sugita S (2007a) Theory of quantitative reconstruction of vegetation I: pollen from large sites REVEALS regional vegetation composition. The Holocene 17 (2):229-241. doi:10.1177/0959683607075837

Sugita S (2007b) Theory of quantitative reconstruction of vegetation II: all you need is LOVE. The Holocene 17 (2):243-257. doi:10.1177/0959683607075838

Suresh PO, Dosseto A, Handley HK, Hesse PP (2014a) Assessment of a sequential phase extraction procedure for uranium-series isotope analysis of soils and sediments. Applied Radiation and Isotopes 83 Pt A:47-55. doi:10.1016/j.apradiso.2013.10.013

Suresh PO, Dosseto A, Hesse PP, Handley HK (2013) Soil formation rates determined from uranium-series isotope disequilibria in soil profiles from the southeastern Australian highlands. Earth and Planetary Science Letters 379:26-37. doi:10.1016/j.epsl.2013.08.004

Suresh PO, Dosseto A, Hesse PP, Handley HK (2014b) Very long hillslope transport timescales determined from uranium-series isotopes in river sediments from a large, tectonically stable catchment. Geochimica et Cosmochimica Acta 142:442-457. doi:10.1016/j.gca.2014.07.033

Tankersley KB, Conover DG, Lentz DL, Callihan A, Weakley J, Hassett I, Platt E, Laiveling A, Bradford E (2019) The impact of maize (Zea mays) on the stable carbon isotope values of archaeological soil organic matter. J Archaeol Sci-Rep 24:324-329. doi:10.1016/j.jasrep.2019.01.024

Tierney JE, Russell JM, Huang YS (2010) A molecular perspective on Late Quaternary climate and vegetation change in the Lake Tanganyika basin, East Africa. Quaternary Science Reviews 29 (5-6):787-800. doi:10.1016/j.quascirev.2009.11.030

Trondman AK, Gaillard MJ, Mazier F, Sugita S, Fyfe R, Nielsen AB, Twiddle C, Barratt P, Birks HJ, Bjune AE, Bjorkman L, Brostrom A, Caseldine C, David R, Dodson J, Dorfler W, Fischer E, van Geel B, Giesecke T, Hultberg T, Kalnina L, Kangur M, van der Knaap P, Koff T, Kunes P, Lageras P, Latalowa M, Lechterbeck J, Leroyer C, Leydet M, Lindbladh M, Marquer L, Mitchell FJ, Odgaard BV, Peglar SM, Persson T, Poska A, Rosch M, Seppa H, Veski S, Wick L (2015) Pollen-based quantitative reconstructions of Holocene regional vegetation cover (plant-functional types and land-cover types) in Europe suitable for climate modelling. Glob Chang Biol 21 (2):676-697. doi:10.1111/gcb.12737

Unkel I, Fernandez M, Björck S, Ljung K, Wohlfarth B (2010) Records of environmental changes during the Holocene from Isla de los Estados (54.4°S), southeastern Tierra del Fuego. Global and Planetary Change 74 (3-4):99-113. doi:10.1016/j.gloplacha.2010.07.003

Valentin C, Poesen J, Li Y (2005) Gully erosion: Impacts, factors and control. CATENA 63 (2):132-153. doi:10.1016/j.catena.2005.06.001

Van Daele M, Moernaut J, Silversmit G, Schmidt S, Fontijn K, Heirman K, Vandoorne W, De Clercq M, Van Acker J, Wolff C, Pino M, Urrutia R, Roberts SJ, Vincze L, De Batist M (2014) The 600 yr eruptive history of Villarrica Volcano (Chile) revealed by annually laminated lake sediments. GSA Bulletin 126 (3-4):481-498. doi:10.1130/b30798.1

Vogel H, Russell JM, Cahyarini SY, Bijaksana S, Watrus N, Rethemeyer J, Melles M (2015) Depositional modes and lake-level variability at Lake Towuti, Indonesia, during the past ~29 kyr BP. Journal of Paleolimnology 54 (4):359-377. doi:10.1007/s10933-015-9857-z

Vogel H, Wagner B, Zanchetta G, Sulpizio R, Rosén P (2010a) A paleoclimate record with tephrochronological age control for the last glacial-interglacial cycle from Lake Ohrid, Albania and Macedonia. Journal of Paleolimnology 44 (1):295-310. doi:10.1007/s10933-009-9404-x

Vogel H, Wessels M, Albrecht C, Stich HB, Wagner B (2010b) Spatial variability of recent sedimentation in Lake Ohrid (Albania/Macedonia). Biogeosciences 7 (10):3333-3342. doi:10.5194/bg-7-3333-2010

Vogel H, Zanchetta G, Sulpizio R, Wagner B, Nowaczyk N (2010c) A tephrostratigraphic record for the last glacial-interglacial cycle from Lake Ohrid, Albania and Macedonia. Journal of Quaternary Science 25 (3):320-338. doi:10.1002/jqs.1311

Wan SM, Toucanne S, Clift PD, Zhao DB, Bayon G, Yu ZJ, Cai GQ, Yin XB, Revillon S, Wang DW, Li AC, Li TG (2015) Human impact overwhelms long-term climate control of weathering and erosion in southwest China. Geology 43 (5):439-442. doi:10.1130/G36570.1

Weber Y, De Jonge C, Rijpstra WIC, Hopmans EC, Stadnitskaia A, Schubert CJ, Lehmann MF, Damste JSS, Niemann H (2015) Identification and carbon isotope composition of a novel branched GDGT isomer in lake sediments: Evidence for lacustrine branched GDGT production. Geochimica Et Cosmochimica Acta 154:118-129. doi:10.1016/j.gca.2015.01.032

Weijers JWH, Schouten S, Spaargaren OC, Damste JSS (2006) Occurrence and distribution of tetraether membrane lipids in soils: Implications for the use of the TEX86 proxy and the BIT index. Organic Geochemistry 37 (12):1680-1693. doi:10.1016/j.orggeochem.2006.07.018

Weltje GJ, Bloemsma MR, Tjallingii R, Heslop D, Röhl U, Croudace IW (2015) Prediction of Geochemical Composition from XRF Core Scanner Data: A New Multivariate

Approach Including Automatic Selection of Calibration Samples and Quantification of Uncertainties. In: Croudace IW, Rothwell RG (eds) Micro-XRF Studies of Sediment Cores: Applications of a non-destructive tool for the environmental sciences. Springer Netherlands, Dordrecht, pp 507-534. doi:10.1007/978-94-017-9849-5_21

Weltje GJ, Tjallingii R (2008) Calibration of XRF core scanners for quantitative geochemical logging of sediment cores: Theory and application. Earth and Planetary Science Letters 274 (3-4):423-438. doi:10.1016/j.epsl.2008.07.054

Wennrich V, Francke A, Dehnert A, Juschus O, Leipe T, Vogt C, Brigham-Grette J, Minyuk PS, Melles M, El'gygytgyn Science P (2013) Modern sedimentation patterns in Lake El'gygytgyn, NE Russia, derived from surface sediment and inlet streams samples. Clim Past 9 (1):135-148. doi:10.5194/cp-9-135-2013

Wennrich V, Minyuk PS, Borkhodoev V, Francke A, Ritter B, Nowaczyk NR, Sauerbrey MA, Brigham-Grette J, Melles M (2014) Pliocene to Pleistocene climate and environmental history of Lake El'gygytgyn, Far East Russian Arctic, based on high-resolution inorganic geochemistry data. Clim Past 10 (4):1381-1399. doi:10.5194/cp-10-1381-2014

White AJ, Stevens LR, Lorenzi V, Munoz SE, Lipo CP, Schroeder S (2018) An evaluation of fecal stanols as indicators of population change at Cahokia, Illinois. Journal of Archaeological Science 93:129-134. doi:10.1016/j.jas.2018.03.009

Wilcken KM, Fujioka T, Fink D, Fulop RH, Codilean AT, Simon K, Mifsud C, Kotevski S (2019) SIRIUS Performance: Be-10, Al-26 and Cl-36 measurements at ANSTO. Nucl Instrum Meth B 455:300-304. doi:10.1016/j.nimb.2019.02.009

Wilhelm B, Sabatier P, Arnaud F (2015) Is a regional flood signal reproducible from lake sediments? Sedimentology 62 (4):1103-1117. doi:10.1111/sed.12180

Willenbring JK, Codilean AT, McElroy B (2013) Earth is (mostly) flat: Apportionment of the flux of continental sediment over millennial time scales. Geology 41 (3):343-346. doi:10.1130/G33918.1

Woodward C, Shulmeister J, Larsen J, Jacobsen GE, Zawadzki A (2014) The hydrological legacy of deforestation on global wetlands. Science 346 (6211):844. doi:10.1126/science.1260510

Yin Q, Berger A (2015) Interglacial analogues of the Holocene and its natural near future. Quaternary Science Reviews 120:28-46. doi:10.1016/j.quascirev.2015.04.008

Zanchetta G, Baneschi I, Francke A, Boschi C, Regattieri E, Wagner B, Lacey JH, Leng MJ, Vogel H, Sadori L (2018) Evidence for carbon cycling in a large freshwater lake in the Balkans over the last 0.5 million years using the isotopic composition of bulk organic matter. Quaternary Science Reviews 202:154-165. doi:10.1016/j.quascirev.2018.10.022

Zell C, Kim JH, Dorhout D, Baas M, Damste JSS (2015) Sources and distributions of branched tetraether lipids and crenarchaeol along the Portuguese continental margin: Implications for the BIT index. Cont Shelf Res 96:34-44. doi:10.1016/j.csr.2015.01.006

Zolitschka B (1998) A 14,000 year sediment yield record from western Germany based on annually laminated lake sediments. Geomorphology 22 (1):1-17. doi:10.1016/S0169-555X(97)00051-2

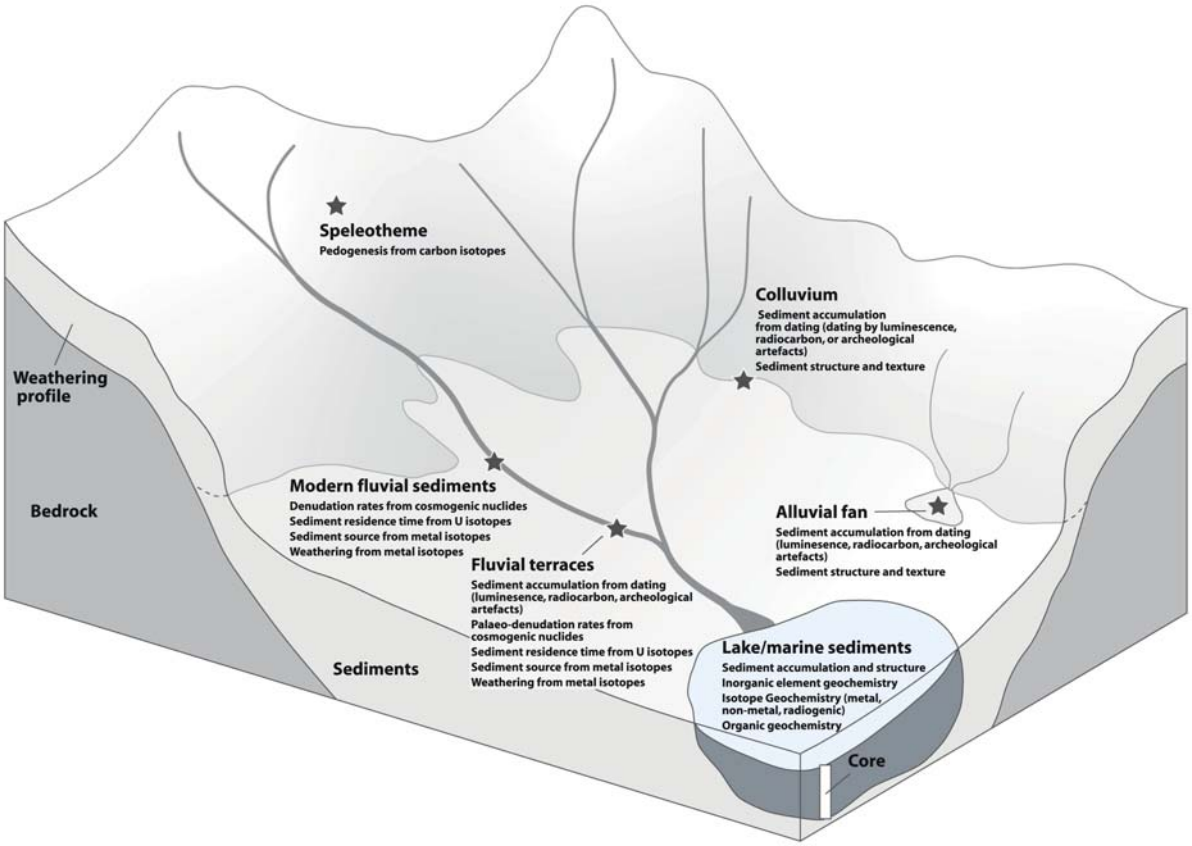
Speleotheme
Pedogenesis from carbon isotopes
Colluvium
Sediment accumulation from dating (dating by luminescence, radiocarbon, or archeological artefacts)
Sediment structure and texture
Weathering profile
Bedrock
Modern fluvial sediments
Denudation rates from cosmogenic nuclides
Sediment residence time from U isotopes
Sediment source from metal isotopes
Weathering from metal isotopes
Alluvial fan
Sediment accumulation from dating (luminesence, radiocarbon, archeological artefacts)
Sediment structure and texture
Fluvial terraces
Sediment accumulation from dating (luminesence, radiocarbon, archeological artefacts)
Palaeo-denudation rates from cosmogenic nuclides
Sediment residence time from U isotopes
Sediment source from metal isotopes
Weathering from metal isotopes
Sediments
Lake/marine sediments
Sediment accumulation and structure
Inorganic element geochemistry
Isotope Geochemistry (metal, non-metal, radiogenic)
Organic geochemistry
Core

Figure 1

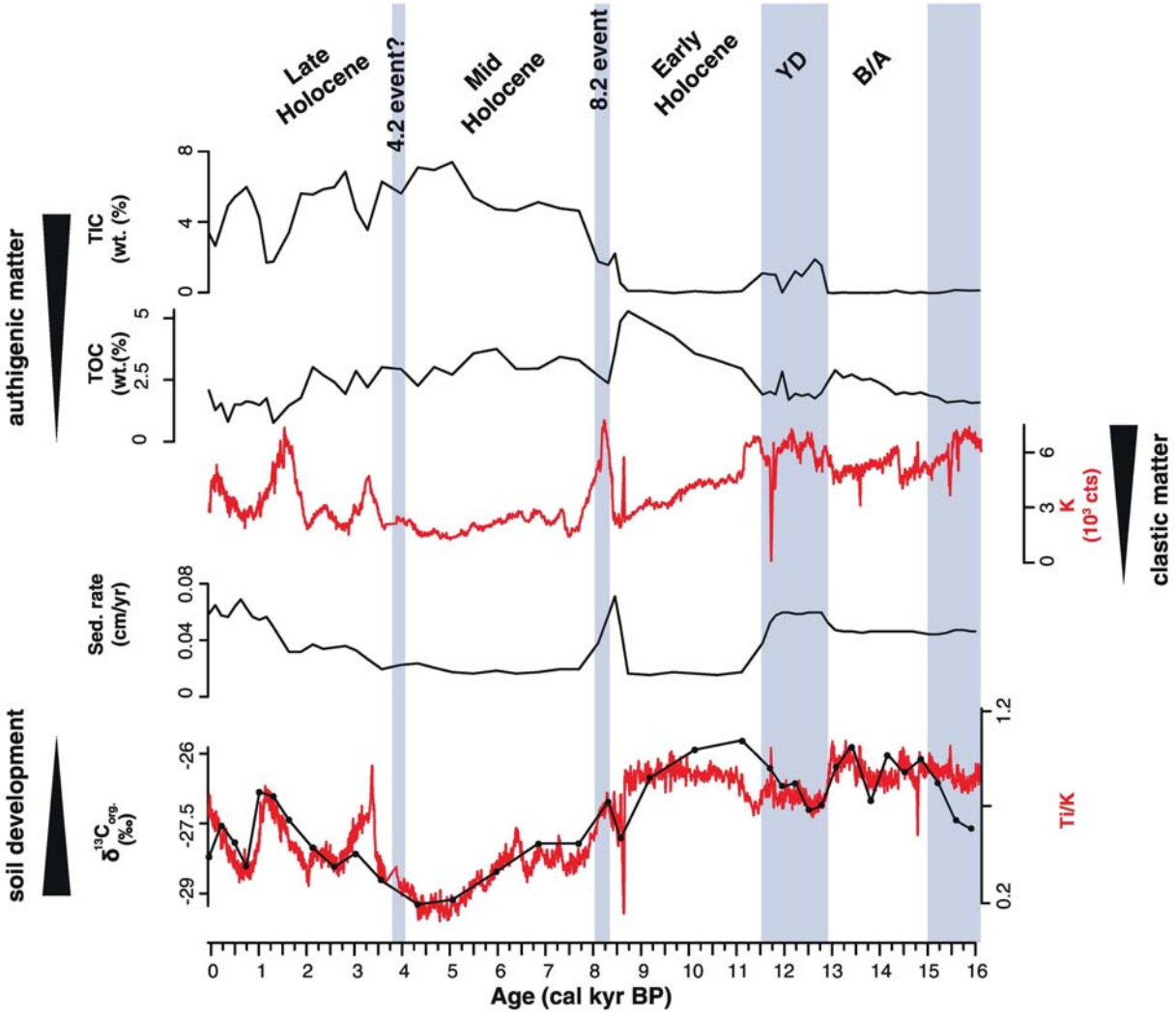
Late Holocene
4.2 event?
Mid Holocene
8.2 event
Early Holocene
YD
B/A
authigenic matter
TIC (wt. (%)
TOC (wt.(%)
Sed. rate (cm/yr)
K (10³ cts)
clastic matter
soil development
δ¹³C org. (‰)
Ti/K
Age (cal kyr BP)

Figure 2

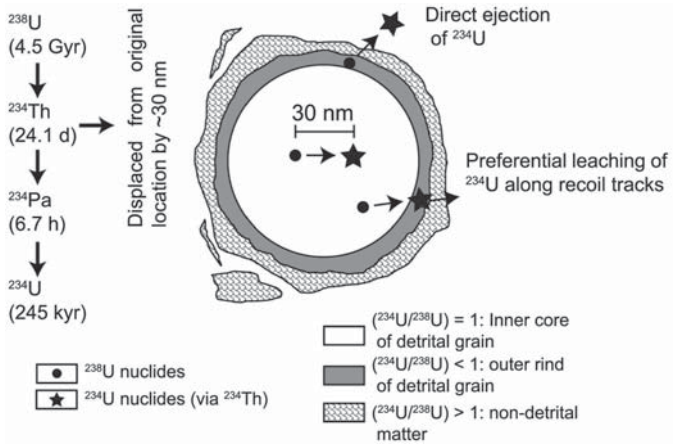
238U
(4.5 Gyr)
234Th
(24.1 d)
234Pa
(6.7 h)
234U
(245 kyr)
Displaced from original location by ~30 nm
Direct ejection of 234U
30 nm
Preferential leaching of 234U along recoil tracks
238U nuclides
234U nuclides (via 234Th)
(234U/238U) = 1: Inner core of detrital grain
(234U/238U) < 1: outer rind of detrital grain
(234U/238U) > 1: non-detrital matter

Figure 3

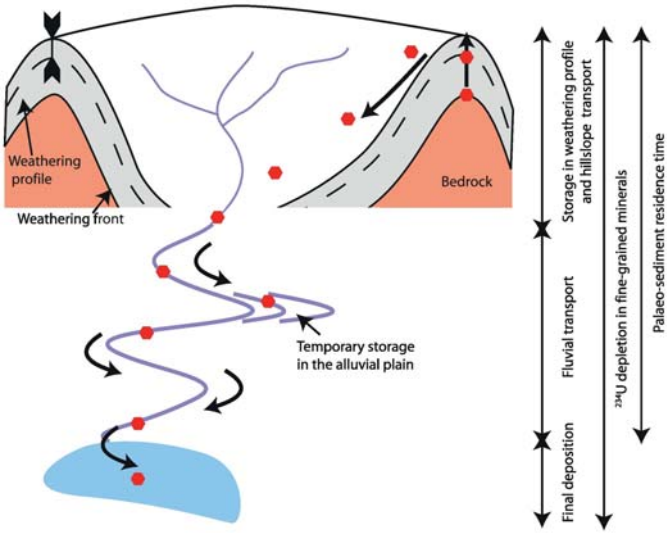
Weathering profile
Weathering front
Bedrock
Temporary storage in the alluvial plain
Storage in weathering profile and hillslope transport
Fluvial transport
Final deposition
^{234}U depletion in fine-grained minerals
Palaeo-sediment residence time

Figure 4

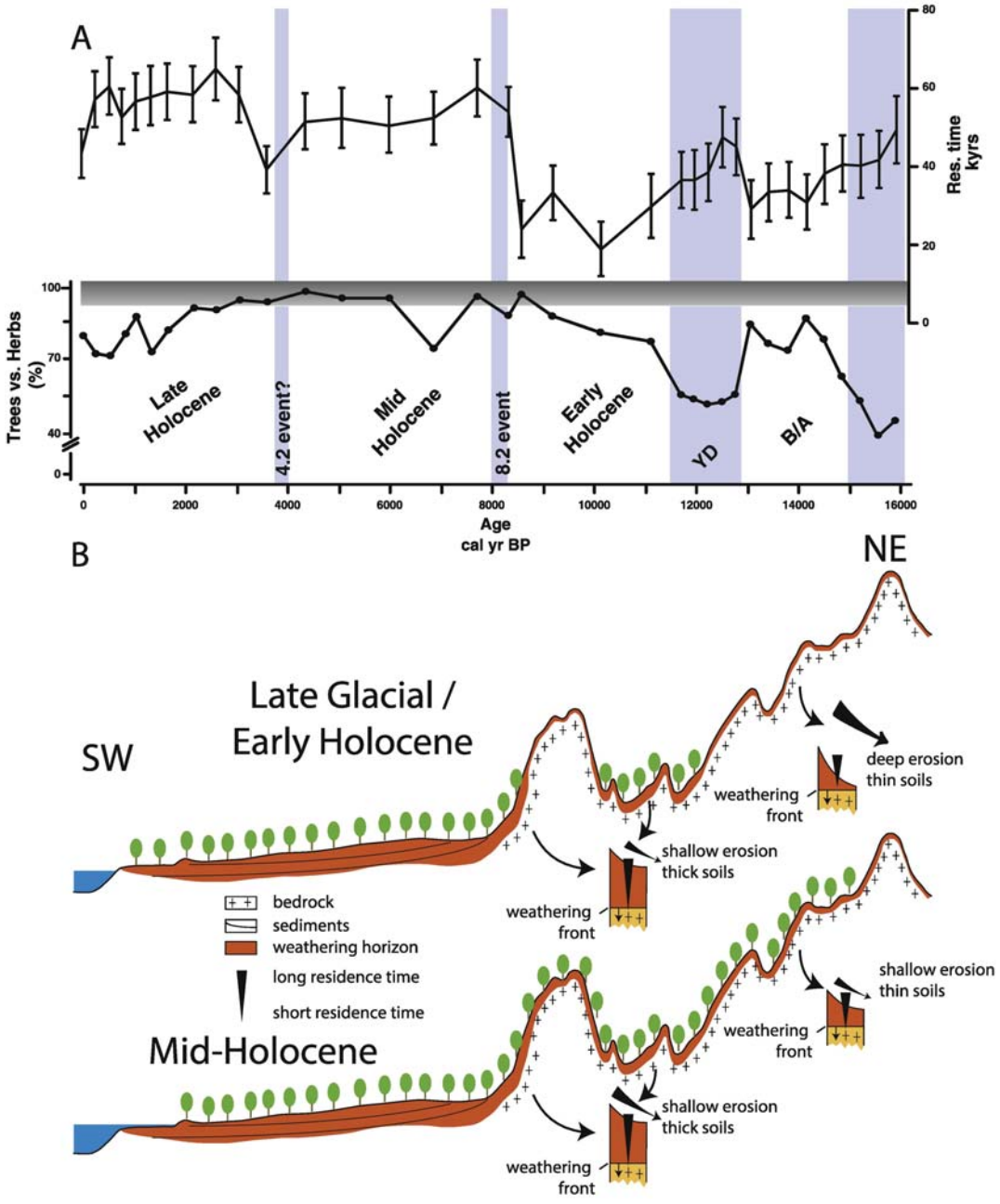
A
Res. time kyrs
Trees vs. Herbs (%)
Late Holocene
4.2 event?
Mid Holocene
8.2 event
Early Holocene
YD
B/A
Age cal yr BP
B
NE
SW
Late Glacial / Early Holocene
deep erosion thin soils
weathering front
shallow erosion thick soils
bedrock
sediments
weathering horizon
long residence time
short residence time
Mid-Holocene
shallow erosion thin soils

Figure 5

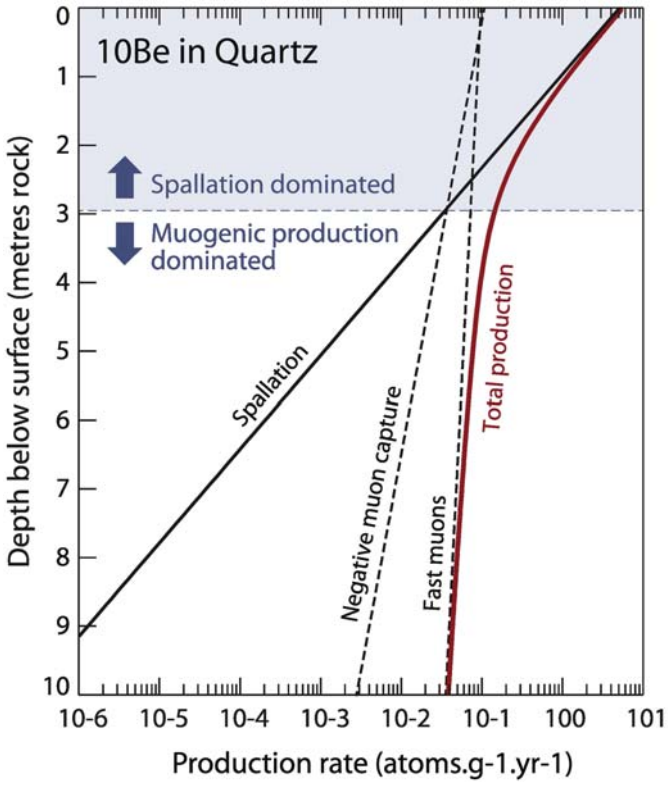
10Be in Quartz
Spallation dominated
Muogenic production dominated
Spallation
Negative muon capture
Fast muons
Total production
Depth below surface (metres rock)
Production rate (atoms.g-1.yr-1)
0
1
2
3
4
5
6
7
8
9
10
10-6
10-5
10-4
10-3
10-2
10-1
100
101

Figure 6

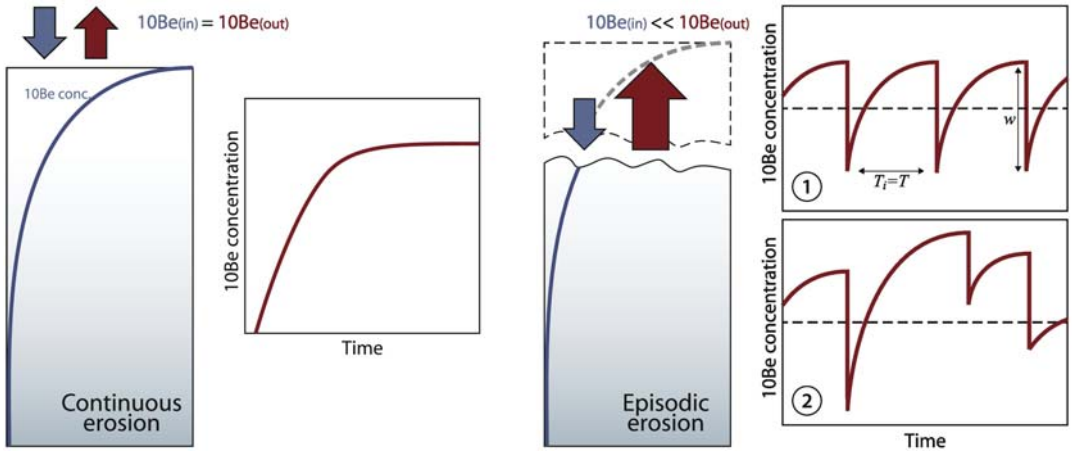
10Be(in) = 10Be(out)
10Be conc.
Continuous erosion
10Be concentration
Time
10Be(in) << 10Be(out)
Episodic erosion
10Be concentration
w
T_i=T
1
10Be concentration
2
Time

Figure 7

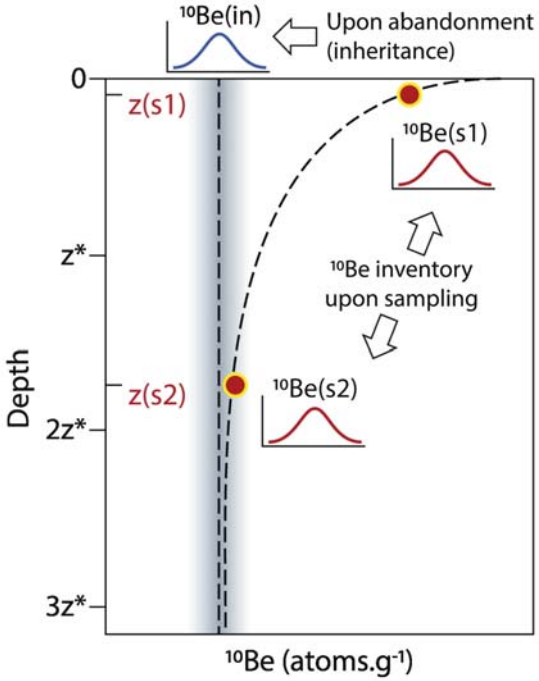
^{10}Be(in)
Upon abandonment
(inheritance)
0
z(s1)
^{10}Be(s1)
z*
^{10}Be inventory
upon sampling
Depth
z(s2)
^{10}Be(s2)
2z*
3z*
^{10}Be (atoms.g^{-1})

Figure 8

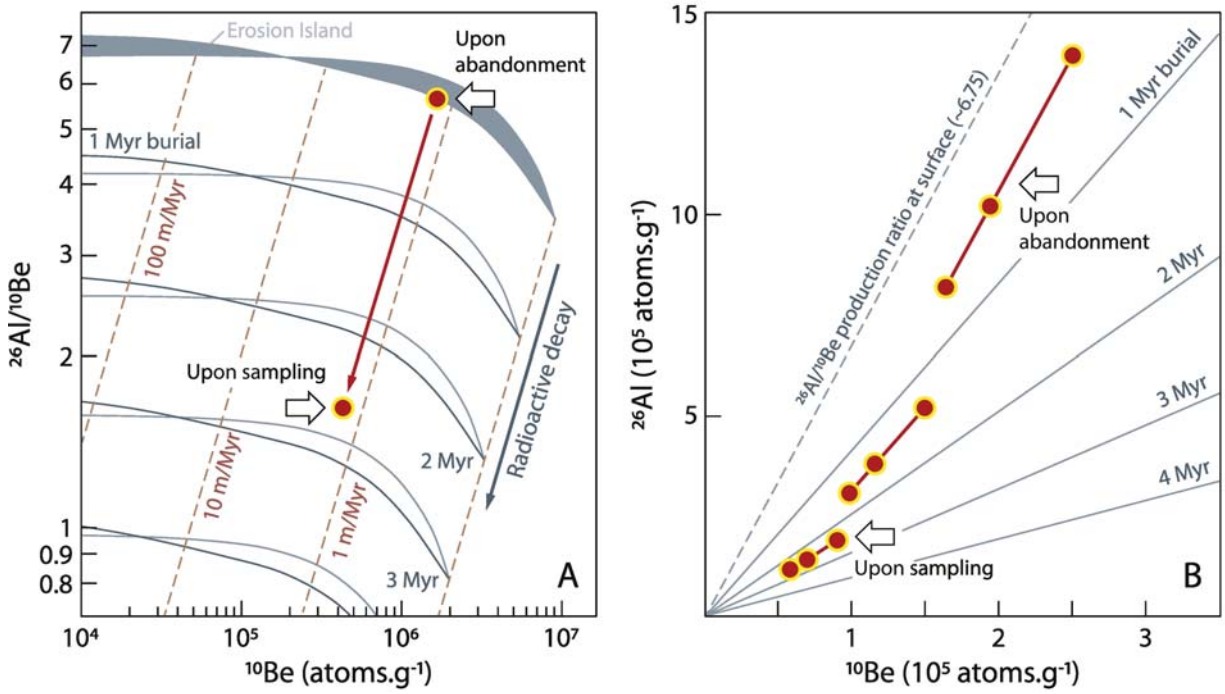
Erosion Island
Upon abandonment
1 Myr burial
100 m/Myr
Upon sampling
10 m/Myr
1 m/Myr
2 Myr
3 Myr
Radioactive decay
A
$^{26}Al/^{10}Be$
^{10}Be (atoms.g^{-1})
$^{26}Al/^{10}Be$ production ratio at surface (~6.75)
1 Myr burial
Upon abandonment
2 Myr
3 Myr
4 Myr
Upon sampling
B
^{26}Al (10^5 atoms.g^{-1})
^{10}Be (10^5 atoms.g^{-1})

Figure 9

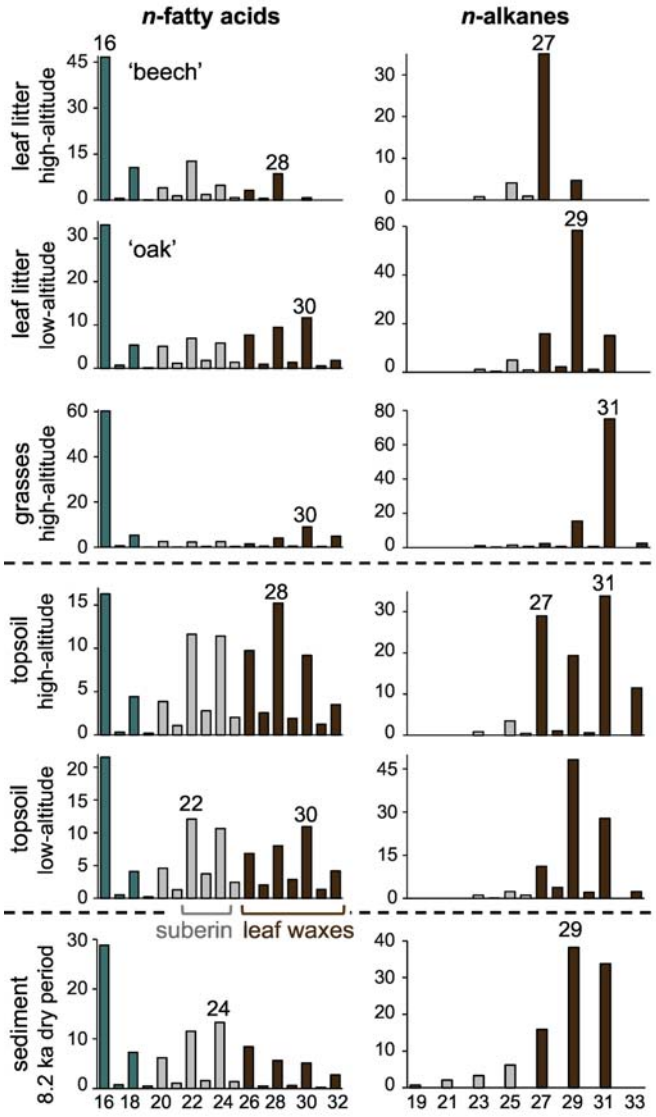
n-fatty acids
n-alkanes
leaf litter high-altitude
'beech'
16
28
27
leaf litter low-altitude
'oak'
30
29
grasses high-altitude
30
31
topsoil high-altitude
28
27
31
topsoil low-altitude
22
30
suberin
leaf waxes
sediment 8.2 ka dry period
24
29
16 18 20 22 24 26 28 30 32
19 21 23 25 27 29 31 33

Figure 10

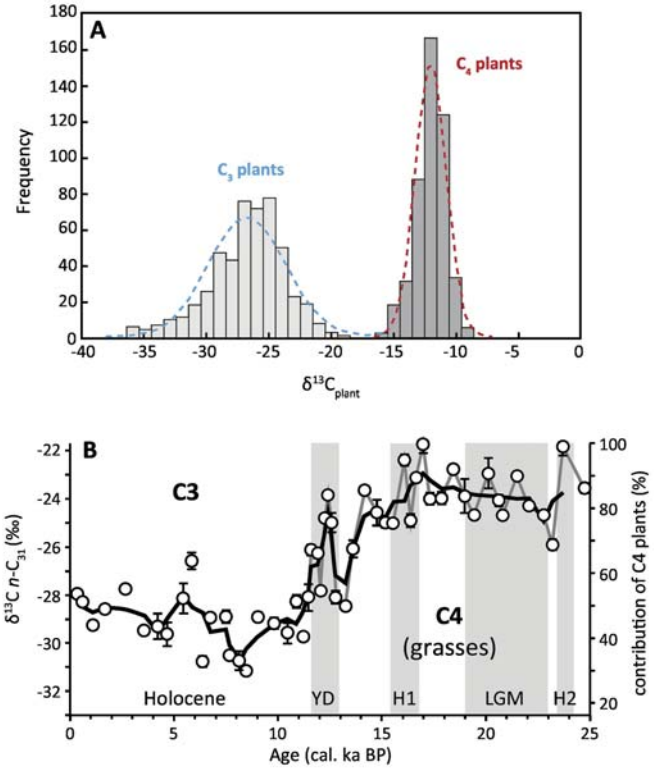
A
Frequency
C_3 plants
C_4 plants
$\delta^{13}C_{plant}$
B
C3
C4
(grasses)
Holocene
YD
H1
LGM
H2
$\delta^{13}C$ n-C_{31} (‰)
contribution of C4 plants (%)
Age (cal. ka BP)

Figure 11